Molecular Therapy
Original Article

Therapeutic Delivery of miR-148a Suppresses Ventricular Dilation in Heart Failure

Andrea Raso,[1,12] Ellen Dirkx,[1,2,12] Leonne E. Philippen,[1,3,12] Amaya Fernandez-Celis,[4] Federica De Majo,[1] Vasco Sampaio-Pinto,[1,5,6,7] Marida Sansonetti,[1] Rio Juni,[1] Hamid el Azzouzi,[1,8] Martina Calore,[1] Nicole Bitsch,[1] Servé Olieslagers,[1] Martinus I.F.J. Oerlemans,[8] Manon M. Huibers,[8] Roel A. de Weger,[8] Yolan J. Reckman,[9] Yigal M. Pinto,[9] Lorena Zentilin,[2] Serena Zacchigna,[2,10] Mauro Giacca,[2,10] Paula A. da Costa Martins,[1,11] Natalia López-Andrés,[4] and Leon J. De Windt[1]

[1]Department of Cardiology, CARIM School for Cardiovascular Diseases, Maastricht University, Maastricht, the Netherlands; [2]International Centre for Genetic Engineering and Biotechnology (ICGEB), Trieste, Italy; [3]Cardiovascular Research Institute, Baylor College of Medicine, Houston, TX, USA; [4]Cardiovascular Translational Research, Navarrabiomed, Instituto de Investigación Sanitaria de Navarra (IdiSNA), Pamplona, Spain; [5]Instituto de Investigação e Inovação em Saúde (i3S), Porto, Portugal; [6]Instituto Nacional de Engenharia Biomédica (INEB), Porto, Portugal; [7]Instituto de Ciências Biomédicas de Abel Salazar (ICBAS), Universidade do Porto, Porto, Portugal; [8]Departments of Cardiology and Pathology, University Medical Center Utrecht, Utrecht, the Netherlands; [9]Department of Experimental Cardiology, Amsterdam UMC location AMC, Amsterdam, the Netherlands; [10]Department of Medicine, Surgery and Health Sciences, University of Trieste, Italy; [11]Department of Physiology and Cardiothoracic Surgery, Faculty of Medicine, University of Porto, Porto, Portugal

Heart failure is preceded by ventricular remodeling, changes in left ventricular mass, and myocardial volume after alterations in loading conditions. Concentric hypertrophy arises after pressure overload, involves wall thickening, and forms a substrate for diastolic dysfunction. Eccentric hypertrophy develops in volume overload conditions and leads wall thinning, chamber dilation, and reduced ejection fraction. The molecular events underlying these distinct forms of cardiac remodeling are poorly understood. Here, we demonstrate that *miR-148a* expression changes dynamically in distinct subtypes of heart failure: while it is elevated in concentric hypertrophy, it decreased in dilated cardiomyopathy. In line, antagomir-mediated silencing of *miR-148a* caused wall thinning, chamber dilation, increased left ventricle volume, and reduced ejection fraction. Additionally, adeno-associated viral delivery of *miR-148a* protected the mouse heart from pressure-overload-induced systolic dysfunction by preventing the transition of concentric hypertrophic remodeling toward dilation. Mechanistically, *miR-148a* targets the cytokine co-receptor glycoprotein 130 (gp130) and connects cardiomyocyte responsiveness to extracellular cytokines by modulating the Stat3 signaling.

These findings show the ability of *miR-148a* to prevent the transition of pressure-overload induced concentric hypertrophic remodeling toward eccentric hypertrophy and dilated cardiomyopathy and provide evidence for the existence of separate molecular programs inducing distinct forms of myocardial remodeling.

INTRODUCTION

Heart failure is a major cause of morbidity and death with little recent progress to reduce its high mortality. This disease is preceded by ventricular remodeling, changes in left ventricular mass, and volume of the myocardium in response to alterations in loading conditions, with two distinct outcomes. Concentric hypertrophy results from cardiac growth and wall thickening, which arises from pressure overload situations on the heart, as observed in patients with chronic hypertension, aortic valve stenosis, or inherited forms of hypertrophic cardiomyopathy, and often yields a substrate for left ventricular diastolic dysfunction.[1,2] Contrary, eccentric hypertrophy often develops under conditions of volume overload of the myocardium, with mitral and aortic regurgitation or familial dilated cardiomyopathy as clinical correlates, resulting in pronounced systolic dysfunction and a concomitant decrease in ejection fraction.[2] Pathological forms of concentric hypertrophy in certain hypertensive or aortic stenosis patients in time may gradually lead to eccentric remodeling of the heart and worsening prognosis.[3] Despite this spectrum of clinically relevant cardiac remodeling phenotypes, the molecular events that underlie these distinct forms of cardiac hypertrophy still remain poorly understood.[4] Accordingly, the stimulatory circulatory agonists, membrane-bound receptors, and intracellular signaling cascades that connect biomechanical forces and the activation of myocardial stress pathways are central to understanding the initiation and progression to concentric versus eccentric hypertrophy.

Cardiotrophin-1 (CT-1), a member of the interleukin-6 (IL-6) cytokine superfamily, exerts its pleiotropic functions using a gp130 homodimer or gp130-leukemia inhibitory factor receptor-β (LIFRβ) heterodimer, induces eccentric hypertrophy in cultured primary

Received 8 January 2018; accepted 11 November 2018;
https://doi.org/10.1016/j.ymthe.2018.11.011.

[12]These authors contributed equally to this work.

Correspondence: Leon J. De Windt, PhD, Department of Cardiology, CARIM School for Cardiovascular Diseases, Maastricht University, Maastricht, the Netherlands.
E-mail: l.dewindt@maastrichtuniversity.nl

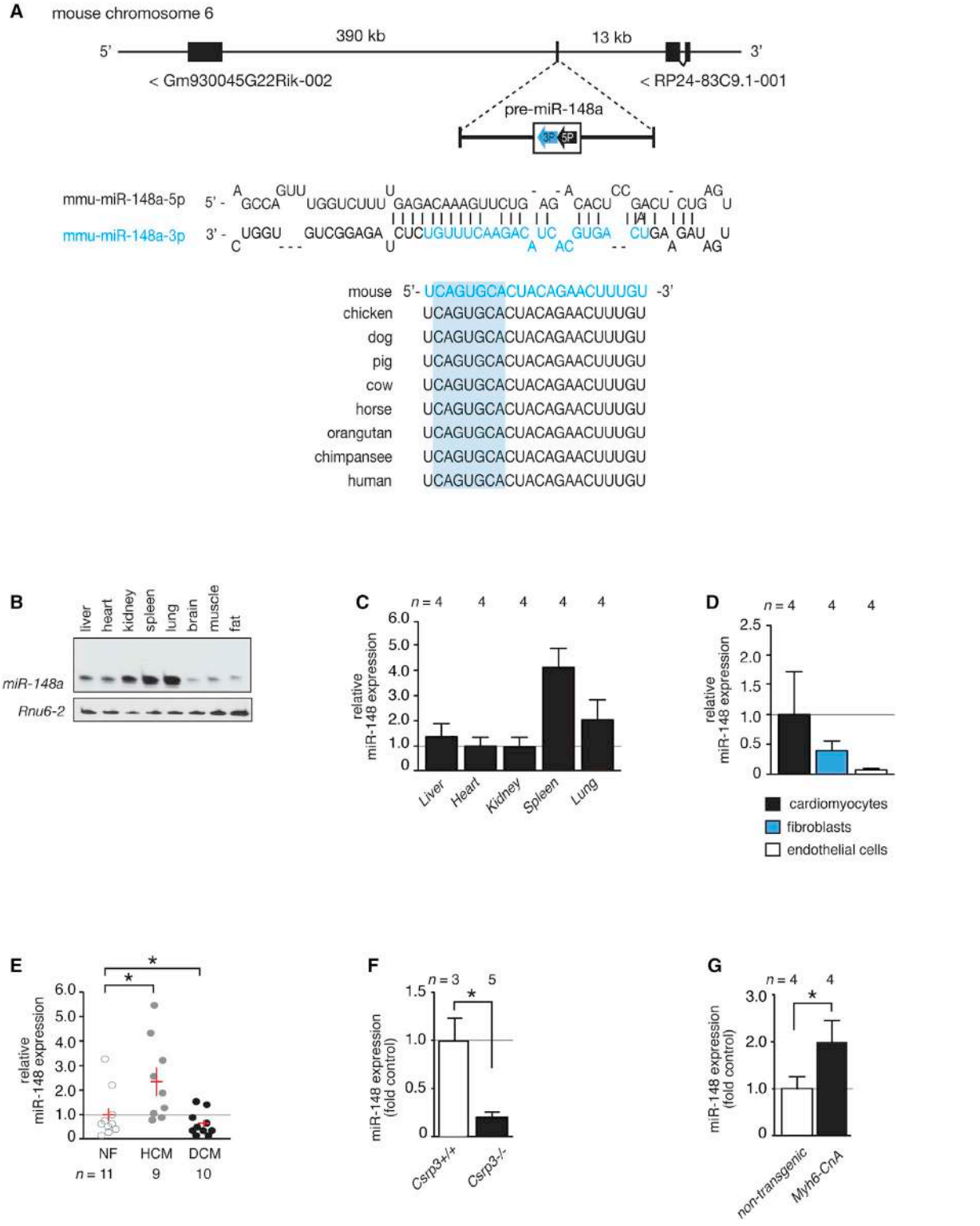

Figure 1. *miR-148a* Shows Dynamic Expression Patterns in Distinct Forms of Heart Failure

(A) Schematic representation of the genomic localization and precursor sequence of *mmu-miR-148a* located on the opposite strand on chromosome 6 in the mouse genome. The mature *miR-148a-3p* strand is conserved among several species. (B) Northern blot analysis of *miR-148a-3p* expression in diverse mouse organs. (C) RT-PCR

(legend continued on next page)

cardiomyocytes *in vitro*[5–7] and exerts cardioprotective proliferative and survival effects in cultured embryonic, neonatal, or adult cardiomyocytes.[8–11] *In vivo*, CT-1 treatment induces left ventricular dilation in rats.[12] In humans, increased CT-1 serum levels are observed in patients with unstable angina,[13] acute myocardial infarction,[14] hypertension, valvular diseases, or heart failure,[15] correlated with the degree of left ventricular systolic dysfunction[16,17] and left ventricular mass index in patients with dilated cardiomyopathy.[18,19]

Cytokines of the IL-6 superfamily couple to gp130 receptors and confer a level of cellular protection against cell death mechanisms in a variety of cardiac stress conditions, and genetic deletion strategies of gp130 or downstream signaling components render widespread cell death in the myocardium in response to biomechanical stress.[20–22] On the other hand, unrestrained activation of cytokine-gp130 signaling transmits prohypertrophic cues that facilitate the transition to eccentric hypertrophy and systolic dysfunction,[23] suggesting that the expression of gp130 is determinant in the balance between cellular survival pathways versus maladaptive hypertrophic remodeling in the myocardium.

Here, we demonstrate that cardiac expression of *miR-148a* alters dynamically in distinct subtypes of human and mouse forms of heart failure. In human and mouse forms of concentric hypertrophy, *miR-148a* expression is elevated, while forms of dilated cardiomyopathy are accompanied by profoundly decreased *miR-148a* myocardial expression. In the heart, *miR-148a* targets gp130 and determines the extracellular cytokines responsiveness and cardiac signaling strength of canonical STAT3 hypertrophic signaling by altering the abundance of gp130. These findings provide evidence that myocardial *miR-148a* functions to prevent the transition of pressure-overload induced concentric hypertrophic remodeling toward eccentric hypertrophy and are proof of the existence of separable molecular cues that provoke distinct forms of hypertrophy in the early steps toward end-stage heart failure.

RESULTS

miR-148a Is Dynamically Expressed in Heart Failure Subtypes

From previous microRNA profiling studies in human cardiac biopsies and mouse cardiac disease models, we observed that *miR-148a-3p* displayed opposite expression patterns depending on the type of heart disease studied.[24] *miR-148a* is an intergenic microRNA, located on chromosome 6 or 7 in the murine and human genome, respectively, and distantly flanked by lncRNA genes (Figure 1A). The major mature *miR-148a* form in the heart is *miR-148a-3p*, which is fully conserved from the mouse to human genome, indicating an evolutionary pressure to resist variations in this microRNA gene (Figure 1A). Northern blotting revealed that *miR-148a* is broadly expressed in various tissues, with a relatively high expression in kidney, spleen, and lung, to a lesser extent in liver and heart, and with traces of expression in brain, muscle, and fat tissue (Figure 1B). In the heart, *miR-148a* is most abundantly expressed in cardiomyocytes and fibroblasts (Figure 1D). Most remarkable, *miR-148a* displayed an opposite direction of differential expression in human cardiac biopsies of end-stage heart failure obtained upon heart transplantation, with a pronounced decrease of *miR-148a* in left ventricular biopsies of dilated cardiomyopathy compared to healthy controls (Figure 1E), compared to an increased expression of *miR-148a* in the left ventricular myocardium of patients with hypertrophic cardiomyopathy compared to the respective healthy controls (Figure 1E). Next, we compared cardiac *miR-148a* expression differences in mouse models of dilated or hypertrophic cardiac remodeling. Cysteine and glycine-rich protein 3 (*Csrp3*), also known as muscle LIM protein, is a Z disc protein involved in cardiac mechanical stretch sensing and required for proper cardiac geometry, energy metabolism, and function. Mice homozygous null for *Csrp3* develop early-onset dilated cardiomyopathy and have been extensively used to study the pathophysiology of this subtype of heart failure. *Csrp3* null mice displayed a very strong reduction of *miR-148a* in left ventricular tissue (Figure 1F). In contrast, mice harboring a constitutively activated mutant of calcineurin A (CnA) under control of the myosin heavy-chain promoter (Myh6-CnA) develop severe hypertrophic concentric remodeling soon after birth. Hearts from young Myh6-CnA mice revealed an increase in *miR-148a* expression (Figure 1G). Taken together, cardiac *miR-148a* expression is increased in human and mouse forms of concentric hypertrophic cardiac remodeling and decreased in human and mouse forms of eccentric remodeling or dilated cardiomyopathy.

miR-148a Targets Cardiac Glycoprotein 130

MicroRNAs exert their action by regulating gene expression at the post-transcriptional level by imperfect base pairing with protein-coding transcripts. Hence, to understand the mechanistic role of *miR-148a* in cardiac remodeling, we first performed a bioinformatic analysis aimed at identifying *miR-148a* binding sites in cardiac expressed protein-coding transcripts. We identified an enrichment of three putative *miR-148a* seed regions in IL-6 signal transducer (*Il6st*), better known as glycoprotein 130 (gp130), and among them, the more proximal *miR-148a* binding site in the ~2.5 kb gp130 3′ UTR demonstrated a perfect match for the *miR-148a* heptametrical seed sequence and showed complete evolutionary conservation (Figure 2A; Figures S2A and S2B). The gp130 co-receptor couples the

analysis of *miR-148a-3p* expression in diverse mouse organs. (D) RT-PCR analysis of *miR-148a-3p* expression in isolated cardiomyocytes, fibroblasts, and endothelial cells from adult mouse hearts. (E) RT-PCR analysis of *miR-148a-3p* expression in human non-failing (control) hearts, human left ventricular myocardium with hypertrophic cardiomyopathy, or human left ventricular myocardium with dilated cardiomyopathy. (F) RT-PCR analysis of *miR-148a-3p* expression in hearts from wild-type and *Csrp3* knockout mice, the gene encoding muscle LIM protein (MLP). (G) RT-PCR analysis of *miR-148a-3p* expression in hearts from 3-week-old non-transgenic littermates and Myh6-CnA transgenic mice. Data are means ± SEM. One-way ANOVA with Bonferroni's multiple-comparison test or Student's paired two-tailed t test was used to compare groups. n, number of hearts; NF, non-failing; DCM, dilated cardiomyopathy; HCM, hypertrophic cardiomyopathy; *Csrp3*, cysteine and glycine-rich protein 3; Myh6, alpha myosin heavy chain; CnA, calcineurin. *$p < 0.05$ versus corresponding control group.

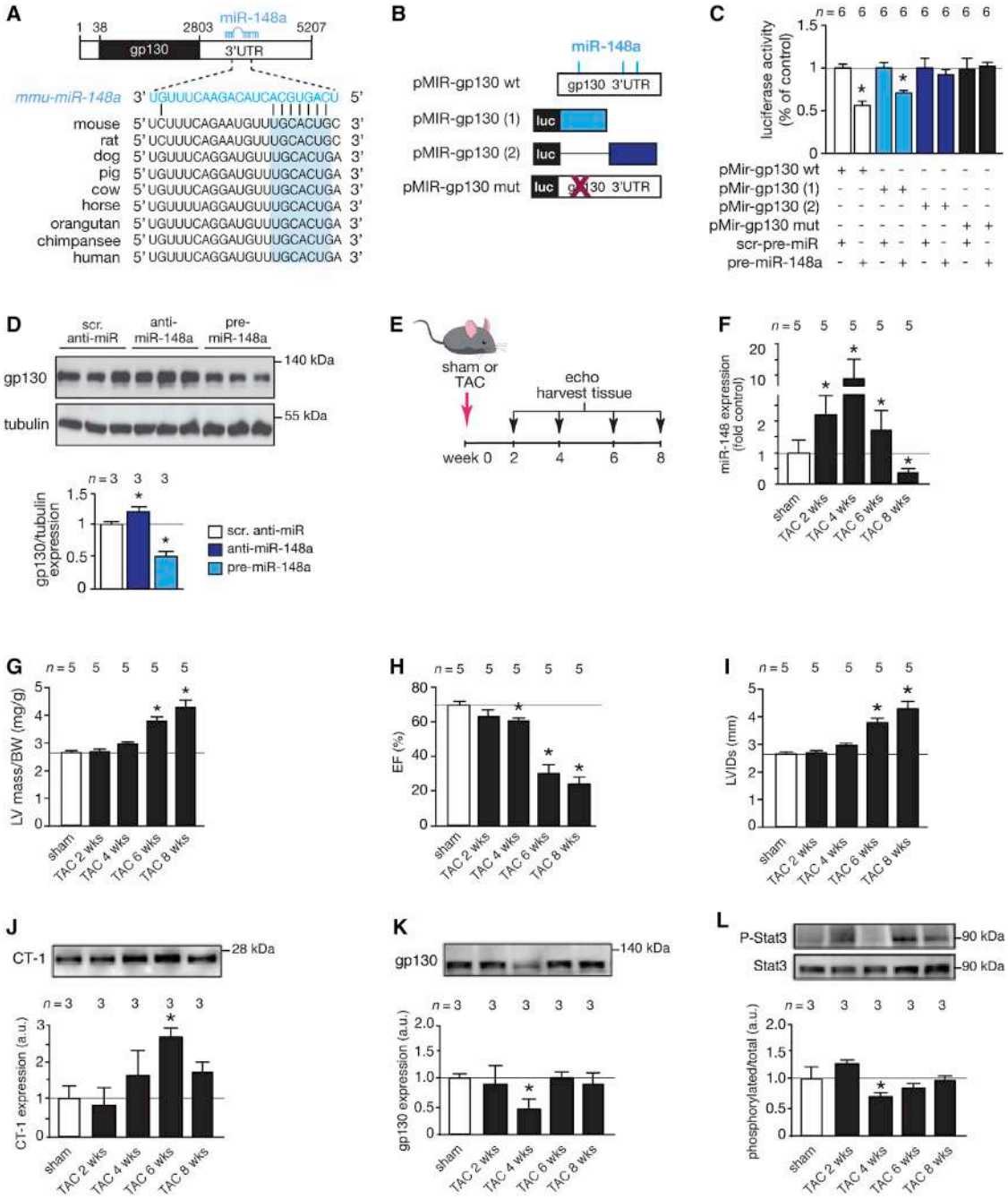

Figure 2. *miR-148a* Targets gp130 and Differentially Regulates gp130 Downstream Signaling in Concentric and Eccentric Cardiac Remodeling

(A) Location and evolutionary conservation of the *mmu-miR-148a* seed region on gp130 3′ UTR (Ensemble: ENSMUST00000183663.7). (B) Schematic representation of luciferase reporter constructs. (C) Activity assay of luciferase reporter constructs in Cos7 cells. (D) Western blot for endogenous gp130 in neonatal rat cardiomyocytes when transfected with scrambled control antimir (scr.anti-miR), antimir-148a (anti-miR-148a), or precursor for *miR-148a* (pre-miR-148a) and quantification of tubulin-corrected gp130 western blot signals. (E) Design of the study: 2-month-old mice were subjected to sham or TAC surgery for 2, 4, 6, or 8 weeks. Mice were subjected to echocardiographic evaluation and hearts harvested at indicated time points. (F) RT-PCR analysis of *miR-148a-3p* expression at indicated time points. (G–I) Echocardiographically determined LV mass divided by BW (G), EF (H), or LVIDs (I), respectively. (J) Western blot analysis of myocardial CT-1 expression and quantification at indicated time points. (K) Western blot analysis of myocardial gp130 expression and quantification at indicated time points. (L) Western blot analysis of myocardial phosphorylated and

(legend continued on next page)

responsiveness of the heart to cytokines from the IL-6 family, including IL-6, LIF, oncostatin M (OSM), or CT-1, and intracellular MAPK, phosphatidylinositol 3-kinase (PI3K), or JAK/STAT signaling by homodimerization or heterodimerization with LIF receptors at the cell surface.[25]

To more directly establish the regulation of gp130 by *miR-148a* in the myocardium, we generated series of luciferase reporters harboring either the complete or truncated forms of the gp130 3′ UTR, including a reporter with site-directed mutagenesis of key nucleotides in the *miR-148a* binding site (Figure 2B). Transient transfection of synthetic precursor *miR-148a* in cultured Cos7 cells decreased gp130 3′ UTR reporter activity when either the intact ~2.5 kb 3′ UTR or a distal truncation was coupled to luciferase compared to co-transfection with scrambled precursor molecules (Figure 2C). In contrast, a proximal truncation of the gp130 3′ UTR, harboring two putative miR-148a binding sites, as well as a site-directed mutant of the complete gp130 3′ UTR, remained unresponsive to synthetic precursor *miR-148a* molecules (Figure 2C). In line, endogenous gp130 protein expression in primary cardiomyocytes was derepressed by transfection of *miR-148a* antimir molecules, while pretreatment with *miR-148a* precursor molecules provoked significant downregulation of endogenous gp130 at the protein level (Figure 2D).

miR-148a Dynamically Influences gp130 Downstream Signaling

miR-148a expression was found increased in forms of concentric hypertrophic cardiac remodeling, while its expression was downregulated in forms of eccentric cardiac remodeling (Figures 1E–1G). To mimic this dynamic expression pattern *in vivo* and study the effects of differential *miR-148a* expression on gp130 expression levels and downstream signaling events in the intact heart, we subjected cohorts of mice to pressure overload by transverse aortic constriction (TAC) surgery, serially assessed cardiac geometry and function and sacrificed mice at 0 weeks (sham) or 2, 4, 6, or 8 weeks after TAC to measure cardiac *miR-148a* expression and evaluate the activation status of signaling cascades (Figures 2E–2L). In line with our previous observations,[24,26,27] concentric hypertrophic remodeling with sustained systolic function was evident in mice in the first 4 weeks following TAC surgery, which gradually transitioned to eccentric remodeling and loss of systolic contractile performance. First, *miR-148a* expression gradually increased up to 10-fold in pressure-overloaded hearts following 2 or 4 weeks of TAC compared to hearts from sham-operated mice (Figure 2F). In this time period, pressure-overloaded hearts increased in heart mass but still displayed sustained systolic function and showed no signs of left ventricular dilation, consistent with concentric hypertrophic remodeling (Figures 2G–2I). More prolonged periods of pressure overload induced a subsequent steep reduction of cardiac *miR-148a* expression, resulting in a significantly lower *miR-148a* expression at 8 weeks of pressure overload compared to sham-operated mice (Figure 2F). Interestingly, at 6 and 8 weeks following TAC, when miR-148a expression steeply reduced, left ventricular mass was clearly increased compared to 2 and 4 weeks after TAC. Additionally, at 6 and 8 weeks following TAC surgery, systolic function was drastically reduced and hearts displayed substantial left ventricular dilation concordant with further eccentric cardiac remodeling compared to 2 and 4 weeks after TAC (Figures 2G–2I). Conclusively, in sustained pressure overload, concentric cardiac remodeling in early phases correlated with high *miR-148a* expression, while eccentric cardiac remodeling in later phases correlated with low expression of *miR-148a*.

Using this model of transient elevation and reduction of *miR-148a* accompanied with a phenotypic switch from concentric to eccentric cardiac remodeling, we assessed expression and activation status of the CT-1/gp130 co-receptor axis. This CT-1/gp130 co-receptor axis has been reported to result in ERK1/2 or ERK5 MAPK, PI3K/Akt, or JAK/STAT3 downstream signaling activation in the heart.[11] Our data show that cardiac CT-1 levels gradually increase in time with the pressure overload stimulus until 6 weeks after TAC, after which this increase ceased (Figure 2J). Interestingly, the expression of the direct *miR-148a* target gene gp130 was reduced by ~50% at week 4 after TAC, a time point that coincides with the highest induction of cardiac *miR-148a* expression (Figure 2K). We also determined the expression of LIF, the LIFR itself, IL-6, ciliary neurotrophic factor (CNTF), and oncostatin M as possible ligands that could all signal through the gp130 co-receptor. No changes in LIF receptor expression were evident during this time period, the expression changes in LIF or OSM remained unchanged or only demonstrated a transient increase at 2 weeks of TAC surgery as was the case for CNTF or IL-6 (Figures S1A and S1E–S1H). These observations lend support to a specificity of the interaction between *miR-148a* and CT-1/gp130 co-receptor axis. A reduction in gp130 expression would be expected to result in ramifications in the activation status of downstream ERK1/2 or ER5 MAPK, PI3K/Akt, or JAK/STAT3 signaling. Indeed, in this model of sustained pressure overloading, a reduction in both phosphorylated STAT3 (Figure 2L) and phosphorylated Akt (Figure S1B), but not total STAT3 or Akt expression, was evident at early time points after TAC, which coincided with the highest induction of cardiac *miR-148a* expression and lowest expression of gp130 (Figures 2F and 2K). No changes in ERK5 or ERK1/2 activation were evident at the time points analyzed (Figures S1C and S1D).

CT-1-mediated gp130 activation and signaling is well known to induce eccentric hypertrophic remodeling and chamber dilatation. Despite clinical and experimental evidence that CT-1 levels are elevated in plasma and myocardium of patients with heart failure, direct evidence that CT-1 is sufficient to promote aspects of cardiac disease *in vivo* is conspicuously lacking in literature. To address

unphosphorylated forms of STAT3 and quantification at indicated time points. Data are means ± SEM. One-way ANOVA with Bonferroni's or Newman-Keul's multiple-comparison test was used to compare groups. n, number of transfection experiments (C), number of transfected wells (D), number of mice (F–L). TAC, transverse aortic constriction; LV mass divided by BW, left ventricular mass to body weight ratio; EF, ejection fraction; LVIDs, left ventricular internal diameter in systole. *$p < 0.05$ versus corresponding control group.

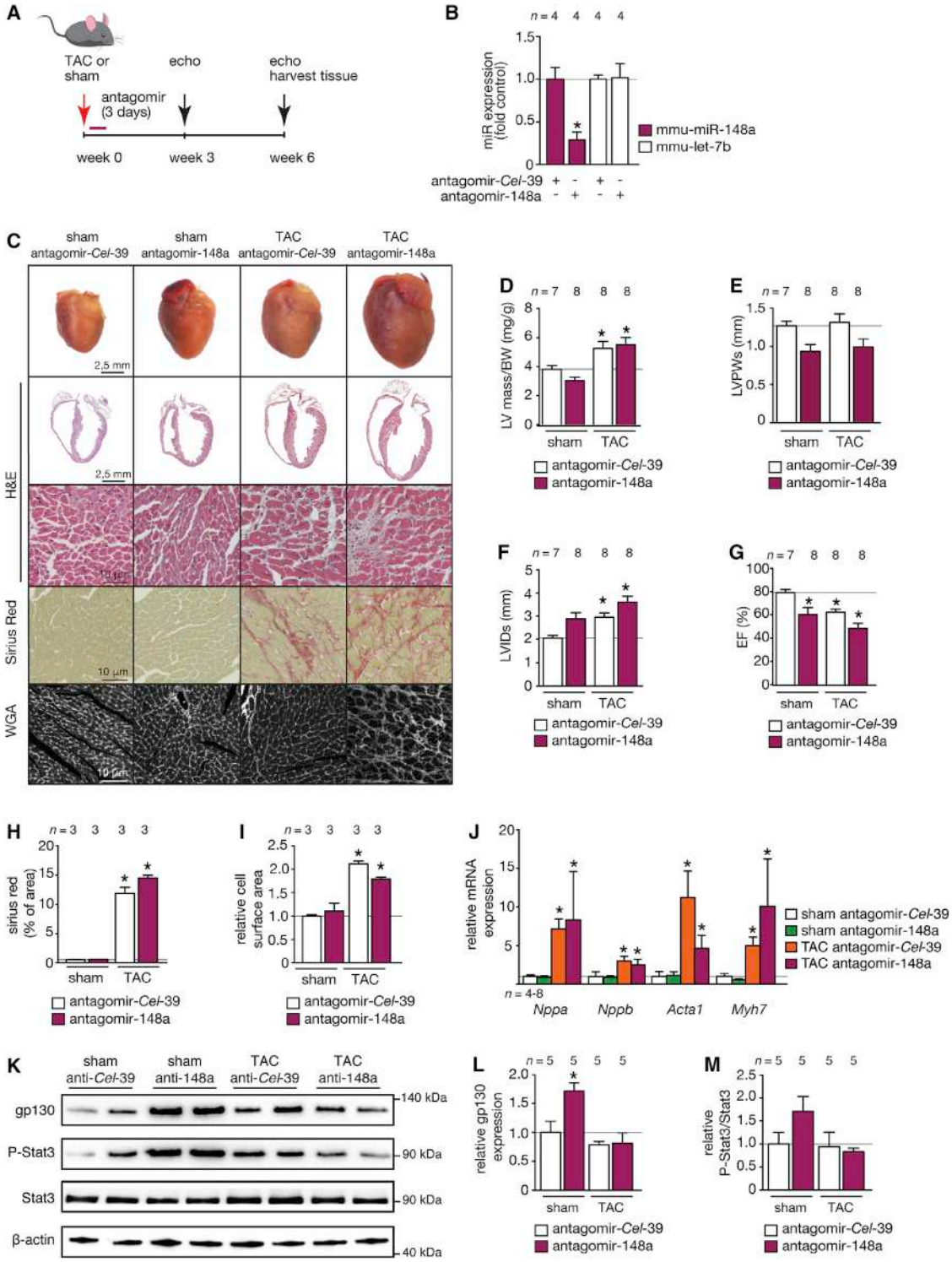

Figure 3. *miR-148a* Silencing Promotes Spontaneous Eccentric Hypertrophic Remodeling and Dilated Cardiomyopathy *In Vivo*

(A) Design of the study. Two-month-old wild-type mice were injected with a control antagomir targeting *C. elegans miR-39* (antagomir-*Cel-39*) or antagomir against *mmu-miR-148a-3p* and subjected to sham or TAC surgery. Cardiac geometry and function was determined by serial Doppler echocardiography at 3 weeks and 6 weeks after surgery. (B) RT-PCR analysis of *miR-148a-3p* and unrelated *let-7b* expression in hearts from mice receiving control antagomir (antagomir-*Cel*-39) or antagomir against

(legend continued on next page)

whether *miR-148a* expression reduces eccentric cardiac remodeling by attenuating gp130 responsiveness to CT-1, we compared cardiac phenotypes of mice that were either left untreated, infused with 20 μg/kg/day of CT-1,[12] or infused with 60 mg/kg/day isoproterenol[28] for 2 weeks (Figure S2C). Our data demonstrate that isoproterenol exposure produced a classical cardiac hypertrophic response accompanied by increased cardiac mass and wall thickening, interstitial fibrosis, and reduced ejection fraction (Figures S2D–S2G). Remarkably, sustained CT-1 exposure produced typical features of eccentric remodeling with mild cardiac enlargement, wall thinning, and severe systolic dysfunction (Figures S2D–S2G). Having established that CT-1 is a direct stimulator of eccentric cardiac remodeling *in vivo*, we observed that primary cardiomyocytes responded to CT-1 with a mild hypertrophic response *in vitro*, which was clearly attenuated by transfection of synthetic precursor *miR-148a* molecules (Figures S2H and S2I). Taken together, these data provide evidence for miR-148a-based regulation of gp130 expression in the adult heart, influencing the responsiveness of the heart to the pro-hypertrophic agonist CT-1.

miR-148a Silencing Provokes Dilated Cardiac Remodeling

To further address the involvement of *miR-148a* in cardiac remodeling, we made use of an antagomir to specifically silence endogenous *miR-148a* expression *in vivo*, a situation that mimics cardiac *miR-148a* reduction as observed in hearts from human and mouse models of dilated cardiomyopathy (Figures 1E and 1F). To this end, we designed chemically modified antisense oligonucleotides to target either *Caenorhabditis elegans miR-39-5p* as control antagomir (antagomir-ctrl or antagomir-*Cel*-39) or *mmu-miR-148a-3p* (antagomir-148a). Antagomirs (80 mg/kg/day) were delivered by intraperitoneal (i.p.) injection on 3 consecutive days to wild-type mice randomized to receive sham or TAC surgery for 6 weeks (Figure 3A). Cardiac *miR-148a* expression was efficiently silenced (Figure 3B).

Remarkably, antagomir-148a treatment sufficed to provoke a mild form of eccentric remodeling with systolic dysfunction in sham-operated mice at 6 weeks after sham operation (Figure 3C). As expected, upon TAC surgery the left ventricular weight (LV)-to-body weight (BW) ratio increased (Figure 3D). As expected, TAC surgery in mice treated with a control antagomir provoked transient hypertrophic remodeling with relatively well-preserved cardiac function at 3 weeks (Table S1). Six weeks of TAC surgery in mice treated with a control antagomir or antagomir-148a resulted in severe myocyte disarray, interstitial fibrosis, systolic and diastolic dysfunction, left ventricular dilation, increased heart weight, as well as an induction of a "fetal" gene program with a tendency of more severe phenotypes in antagomir-148a-treated mice (Figures 3C–3J; Table S2). Next, we analyzed protein levels of gp130 and p-STAT3 by western blotting. The data demonstrate that silencing *miR-148a* in sham-operated mice substantially derepressed (induced) its downstream target gp130 (Figure 3K). As a result, the phosphorylated (activated) form of STAT3 was increased when gp130 was increased in expression (Figure 3K). Total expression levels of STAT3 remained unchanged, indicating activation of STAT3 downstream of gp130 signaling in the heart (Figures 3L and 3M). This result further supports our conclusion that endogenous *miR-148a* expression levels directly target gp130, subsequently resulting in activation of STAT3 signaling in the heart. Taken together, these data demonstrate that *miR-148a* silencing *in vivo* evokes mild cardiac dilation with derepression of gp130 under baseline conditions and mildly exacerbated pressure overload-induced cardiac remodeling and dysfunction.

miR-148a Overexpression Suppresses Pressure Overload-Induced Cardiac Dilation

Next, we mimicked the increased expression of *miR-148a* as observed in conditions of concentric cardiac remodeling in human and mouse hypertrophic cardiomyopathy (Figures 1D and 1F). To this end, we made use of the high cardiac tropism and prolonged expression of viral vectors based on adeno-associated vector serotype9 (AAV9) upon systemic delivery. AAV9 vectors expressing either *mmu-miR-148a* (AAV9-148a) or an empty control vector (AAV9-MCS) were administered intravenously (i.v.) by injection into the internal jugular vein of adult mice (Figure 4A). The hearts of AAV9-148a-injected animals displayed an induction of *miR-148a* of about 2-fold over control (Figure 4B) and appeared morphologically normal, with no signs of cardiomyocyte hypertrophy, changes in collagen content, or induction of a fetal gene program apart from a mild induction of *Nppa* (Figures 4C–4J), indicating that increased *miR-148a* expression alone is not an active driver of cardiac hypertrophy or remodeling *in vivo* in the absence of additional stimuli.

To analyze *miR-148a* cardiac function under pressure-overload conditions, AAV9-148a and AAV9-MCS-treated animals were randomized to receive sham or TAC surgery. Six weeks of TAC surgery in AAV9-MCS mice resulted in increased LV, severe myocyte disarray, interstitial fibrosis, increased cardiomyocyte size, systolic and diastolic dysfunction, left ventricular dilation, as well as an induction of the classical "fetal" gene program (Figures 4C–4J; Tables S3 and

miR-148a. (C) Representative images of whole hearts (top panel), H&E-stained sections of four-chamber view (second panel), high-magnification H&E-stained sections (third panel), Sirius-red-stained sections (fourth panel), and WGA-stained (fifth panel) histological sections. (D) Measurement of LV mass/BW ratio, (E) LVPWs, (F) LVIDs, or (G) EF by echocardiography in antagomir control and antagomir-148a-treated mice after sham or TAC surgery. Measurements of (H) fibrotic area (Sirius red staining) and (I) cell-surface area in control and antagomir-148a-treated mice after sham or TAC surgery. (J) RT-PCR analysis of transcript abundance of the hypertrophic stress marker genes *Nppa*, *Nppb*, *Acta1*, and *Myh7* in hearts from control antagomir or antagomir-148a-treated mice after sham or TAC surgery. (K–M) Western blot analysis (K) and quantification of myocardial gp130 (L) or phosphorylated and unphosphorylated forms of STAT3 (M) in hearts from mice subjected to sham or TAC surgery and receiving antagomir-148a or a control antagomir (antagomir-*Cel*-39). Data are means ± SEM. One-way ANOVA with Bonferroni's or Newman-Keuls multiple-comparison test was used to compare groups. n, number of hearts; TAC, transverse aortic constriction; WGA, wheat germ agglutinin; LV mass/BW, left ventricular mass to body weight ratio; LVPWs, left ventricular posterior wall end systole; LVIDs, left ventricular internal diameter in systole; EF, ejection fraction; *Nppa*, natriuretic peptide type A; *Nppb*, natriuretic peptide type B; *Acta1*, alpha skeletal actin; *Myh7*, beta myosin heavy chain. *$p < 0.05$ versus corresponding control group.

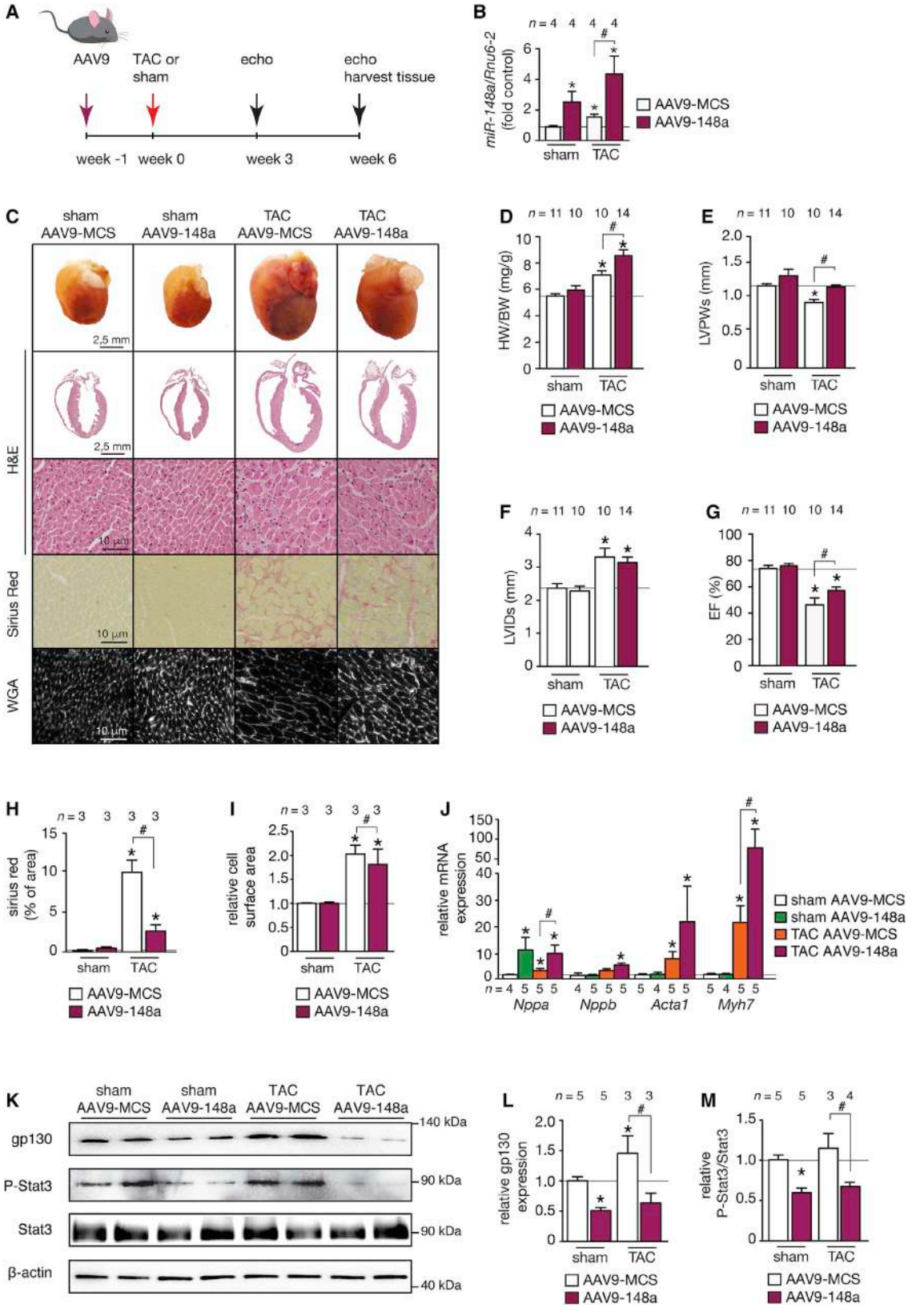

(legend on next page)

S4). In addition, cardiomyocyte apoptosis was increased in TAC samples compared to both sham groups (Figure S4). Strikingly, cardiac histopathology, cardiomyocyte hypertrophy, and systolic function were clearly attenuated in AAV9-148a-injected mice after 6 weeks of TAC surgery (Figures 4C–4J; Table S4). A more pronounced induction of transcripts encoding *Nppa*, *Acta1*, and *Myh7* as part of the "fetal" gene program was observed in hearts from AAV9-148a-injected mice receiving TAC surgery compared to AAV9-MCS-injected mice that received TAC surgery (Figure 4J). Importantly, the extent of cardiomyocyte apoptosis was similar between the two groups receiving TAC surgery (Figure S4).

We also performed western blotting in hearts from the four experimental groups. We probed the membranes with antibodies specific for gp130 or its immediate downstream signal transducer STAT3 to assess phospho-STAT3 and total STAT3 levels. The data demonstrate that overexpression of *miR-148a* substantially reduced the expression of its downstream target gp130 (Figures 4K–4M). As a result, the phosphorylated (activated) form of STAT3 was decreased when gp130 was reduced in expression. Total expression levels of STAT3 remained unchanged, indicating reduced activation status of STAT3 downstream of gp130 signaling in the heart. This result further supports our conclusion that endogenous *miR-148a* controls gp130 expression levels, subsequently resulting in differential activation status of STAT3 in the heart. Conclusively, these data demonstrate that elevation of cardiac *miR-148a* expression *in vivo* protects the myocardium from dilation and cardiac dysfunction following pressure overload, and this suppression was accompanied by the reduction of gp130 signaling.

miR-148a Overexpression Attenuates the Transition of Pressure-Overload-Induced Concentric toward Eccentric Remodeling

Our data indicate a correlation between the dynamic *miR-148a* expression and the distinct phases of cardiac remodeling under sustained pressure-overload conditions, starting from concentric hypertrophy in early phases toward eccentric remodeling in later phases of overload. To more firmly demonstrate the functional significance of lowered *miR-148a* expression in the transition toward eccentric cardiac hypertrophy, we designed a gene therapeutic approach with AAV9-148a, where mice were first randomized to receive sham or TAC surgery for 4 weeks. Next, AAV9 vectors expressing either *mmu-miR-148a* (AAV9-148a) or an empty control vector (AAV9-MCS) were then administered i.v. by injection into the internal jugular vein of adult mice (Figure 5A) to prevent the observed decrease in *miR-148a* in later phases of pressure overload as an approach to maintain high expression of *miR-148a* for another 3 weeks. We confirmed that this approach resulted in higher cardiac *miR-148a* expression in sham-operated AAV9-148a-injected mice (Figure 5B), and these hearts appeared morphologically normalwith no signs of altered cardiac contractile function, cardiomyocyte hypertrophy, changes in collagen content, except for a relatively mild induction of *Nppb* and *Myh7* (Figures 5C–5J).

As expected, at 7 weeks of sustained pressure overload, AAV9-MCS-injected mice displayed reduced LV wall thickness and increased LV dilation accompanied with interstitial fibrosis, increased cardiomyocyte size, systolic dysfunction, as well as an induction of the classical "fetal" gene program (Figures 5C–5J; Tables S5–S7). In contrast, LV wall thickness was maintained, the extent of LV dilation was attenuated, and systolic contractility was clearly improved in AAV9-148a-injected mice at 7 weeks of TAC surgery compared to AAV9-MCS mice receiving TAC surgery (Figures 5C–5G; Table S7). *miR-148a* overexpression also resulted in less fibrotic remodeling (Figure 5H) and a more pronounced induction of "fetal" gene transcripts encoding *Nppb* and *Myh7* (Figure 5J).

Combined, our data reveal that *miR-148a* expression dynamically regulates cardiac gp130 expression and alters the responsiveness of the heart to CT-1 stimulation and downstream STAT3 signaling strength, where relatively high *miR-148a* expression produces forms of concentric hypertrophic remodeling and dampens CT-1 overstimulation that drives deleterious eccentric cardiac remodeling (Figure 5K).

DISCUSSION

Here, we demonstrate that cardiac expression of *miR-148a* alters dynamically in distinct subtypes of human and mouse forms of heart failure, with high *miR-148a* expression in human and mouse forms of concentric hypertrophy and decreased *miR-148a* expression in forms of dilated cardiomyopathy. Mechanistically, *miR-148a* modulates the coupling between extracellular CT-1 and cardiac signaling strength of

Figure 4. Cardiac AAV9-miR-148a Overexpression Protects the Heart against Eccentric Hypertrophy, Chamber Dilation, and Systolic Dysfunction

(A) Design of the study. Two-month-old mice were injected with control AAV9 (AAV9-MCS) or an AAV9 designed to overexpress *mmu-miR-148a-3p* (AAV9-148a) and subjected to sham or TAC surgery. Cardiac geometry and function was determined by serial Doppler echocardiography at 3 and 6 weeks after surgery. (B) RT-PCR analysis of *miR-148a-3p* expression in hearts from mice receiving AAV9-MCS or AAV9-148a virus. (C) Representative images of whole hearts (top panel), H&E-stained sections of four-chamber view (second panel), high-magnification H&E-stained sections (third panel), Sirius-red-stained sections (fourth panel), and WGA-stained (fifth panel) histological sections. (D) Measurements of LV mass/BW ratio, (E) LVPWs, (F) LVIDs, (G) EF, (H) fibrotic area (Sirius red staining), and (I) cell-surface area in AAV9-CMV- and AAV9-148a-treated mice after sham or TAC surgery. (J) RT-PCR analysis of transcript abundance of hypertrophic stress marker genes *Nppa*, *Nppb*, *Acta1*, and *Myh7* in hearts from AAV9-MCS and AAV9-148a-treated mice after sham or TAC surgery. (K–M) Western blot analysis (K) and quantification of myocardial gp130 (L) or phosphorylated and unphosphorylated forms of STAT3 (M) in hearts from mice subjected to sham or TAC surgery and receiving AAV9-148a or AAV9-MCS (MCS, multiple cloning site; empty vector). Data are means ± SEM. One-way ANOVA with Bonferroni's or Newman-Keul's multiple-comparison test was used to compare groups. n, number of hearts; AAV9, adeno-associated vector serotype 9; TAC, transverse aortic constriction; WGA, wheat germ agglutinin; LV mass/BW, left ventricular mass to body weight ratio; LVPWs, left ventricular posterior wall end systole; LVIDs, left ventricular internal diameter in systole; EF, ejection fraction; *Nppa*, natriuretic peptide type A; *Nppb*, natriuretic peptide type B; *Acta1*, alpha skeletal actin; *Myh7*, beta myosin heavy chain. *$p < 0.05$ versus corresponding control group; #$p < 0.05$ versus experimental group.

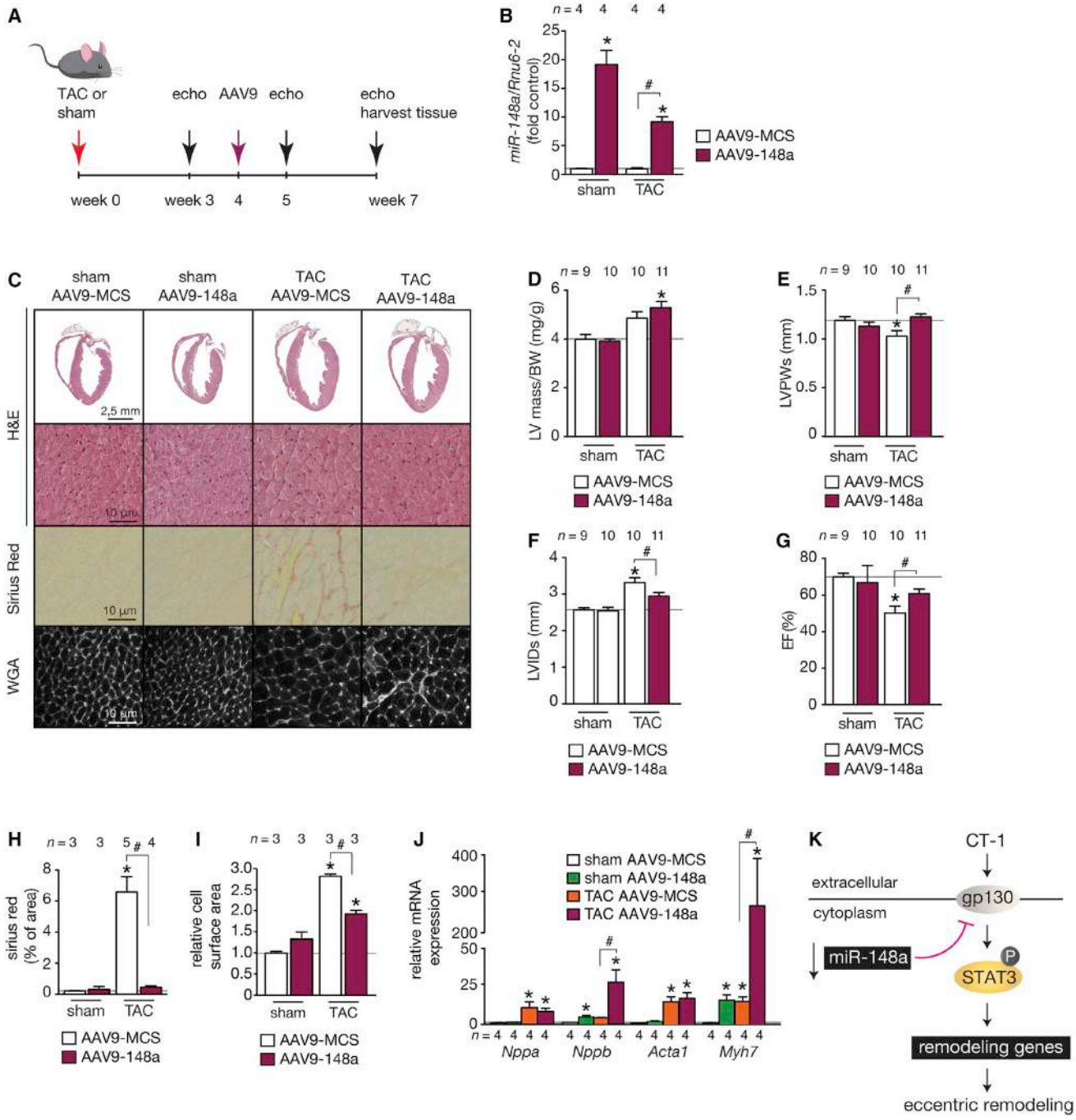

Figure 5. *miR-148a* Overexpression Prevents the Transition of Pressure-Overload-Induced Concentric Hypertrophic Remodeling toward Eccentric Hypertrophy

(A) Design of the study. Two-month-old mice were subjected to sham or TAC surgery and 4 weeks later injected with control AAV9 (AAV9-CMV) or AAV9-148a. Cardiac geometry and function was determined by serial Doppler echocardiography at 3, 5, and 7 weeks after surgery. (B) RT-PCR analysis of *miR-148a-3p* expression in hearts from mice receiving AAV9-CMV or AAV9-148a virus. (C) Representative images of H&E-stained sections of four-chamber view (top panel), high-magnification H&E-stained sections (second panel), Sirius-red-stained sections (third panel), and WGA-stained (fourth panel) histological sections. (D) Measurements of LV mass/BW ratio, (E) LVPWs, (F) LVIDs, (G) EF, (H) fibrotic area (Sirius red staining), and (I) cell surface area in AAV9-CMV and AAV9-148a-treated mice after sham or TAC surgery. (J) RT-PCR analysis of transcript abundance of hypertrophic stress marker genes *Nppa*, *Nppb*, *Acta1*, and *Myh7* in hearts from AAV9-CMV and AAV9-148a-treated mice after sham or TAC surgery. (K) Model depicting the influence of *miR-148a* on the CT-1-gp130-STAT3 signaling axis in cardiac stress situations, resulting in differential activation of STAT3

(legend continued on next page)

the canonical STAT3, Akt, Erk5, and Erk1/2 hypertrophic cascades by targeting gp130, a pivotal co-receptor for cytokines of the IL-6 superfamily.

Using complimentary gain- and loss-of-function studies for *miR-148a* in mouse models for cardiac pressure overload, we demonstrate that the abundance of *miR-148a* and consequently the reduction of gp130 levels connect sustained biomechanical forces to diverse forms myocardial remodeling, with an overall conclusion that *miR-148a* expression acts as a protective molecular driver that promotes wall thickening and concentric remodeling. Here, we used AAVs as a genetic tool to accomplish overexpression of miR-148a. Naturally occurring viruses have evolved to efficiently transduce their genetic information into host cells. Recombinant viral vectors are engineered by replacing non-essential viral genes with foreign genes of therapeutic interest, and used as vehicles for efficient infecting a wide variety of cell types. AAV vectors are increasingly recognized as reliable tool for research purposes due to their low immunogenicity, tissue tropism, and relative safety due to their low rate of genomic integration.[29,30] Specifically, AAV vectors of serotype 1/6/9 (AAV1/6/9) that display varying ranges of cardiac tropism, are used to deliver a variety of therapeutic genes, including small functional non-coding RNAs such as microRNAs. Future improvement of AAV vectors should address their limited capacity to carry transgenes of larger sizes. Likewise, the existence of pre-existing neutralizing antibodies against AAV in the general population hampers immediate translation of AAV cardiac gene therapy to clinical stages. Notwithstanding these drawbacks, AAV vectors can be considered as safe, efficient, and reliable tools for preclinical cardiac gene therapy applications with high potential as vectors in clinical trials. Vice versa, lowering of cardiac *miR-148a* expression results in increased gp130 expression leading to enhanced gp130-coupled intracellular signaling, and incites wall thinning and chamber dilation with the associated increase in stress on the ventricular wall, representing the first irreversible steps toward overt heart failure in dilated cardiomyopathy. Our findings are proof of the existence of separable molecular programs primary to concentric hypertrophy versus eccentric hypertrophy, chamber narrowing versus chamber dilation and wall thickening versus wall thinning, all occurring within the venue of biomechanical driven pathways of cardiac growth and failure.

Cardiac remodeling in patients with heart disease encompass all quantifiable changes in left ventricular mass and volume, with a wide variety in the ratio of left ventricular wall thickness to chamber radius, often referred to as relative wall thickness (RWT) and diagnosed by echocardiographic or cardiac MRI data.[3] A normal left ventricular chamber size refers to normal geometry, while differences in RWT distinguish concentric from normal and from eccentric remodeling. Concentric hypertrophy tends to arise from pressure-overload situations in the heart, as observed in patients with aortic valve stenosis or hypertensive heart diseases, often yielding a substrate for left ventricular diastolic dysfunction. In contrast, eccentric hypertrophy develops secondary to conditions of volume overload of the myocardium, clinically observed in mitral and aortic regurgitation, precipitating in a strong reduction of ejection fraction.[3] Despite the existence of a relatively detailed clinical diagnosis and physiological underpinnings of this spectrum of clinically relevant remodeling phenotypes, the molecular events that underlie distinct forms of cardiac hypertrophy still remain poorly charted.[31] Accordingly, the stimulatory circulatory agonists, membrane-bound receptors, and intracellular signaling cascades that connect biomechanical forces and the activation of myocardial stress pathways are central to understanding the initiation and progression to concentric hypertrophy as clinically observed in hypertrophic cardiomyopathies versus eccentric hypertrophy as it occurs in forms of dilated cardiomyopathy.

In cultured cardiomyocytes, CT-1 signals through a gp130 homodimer or gp130/LIFRβ heterodimer. Moreover, it was reported to induce a peculiar form of hypertrophy with increased cardiomyocyte size, consisting on an increase in cell length but no significant change in cell width, due to the assembly of sarcomeric units in series, as is more commonly observed upon stimulation with the canonical pro-hypertrophic adrenergic agonists or endothelin-1.[6,7] The involvement of ERK5 and STAT3 in CT-1-induced longitudinal elongation has been reported in adult cardiomyocytes[7] and it is further supported by the molecular observation that overexpression of activated ERK5 induces serial insertion of sarcomeres in neonatal cardiomyocytes *in vitro*.[32] Interestingly, STAT3 upregulates ERK5 in other cell types. Thus, the possibility that STAT3 mediates the longitudinal elongation through the downstream activation of ERK5, which determines cardiomyocyte elongation, requires further investigations.

These morphological differences find a basis in the activation of distinct signaling cascades and proteomic outcomes between cytokines from the IL-6 superfamily or endothelin-1.[33] Elongated cardiomyocytes, myocardial dilation, and decreased ejection fraction were also evident following 6 weeks of CT-1 treatment in rats.[7] In line, in the current study we developed and characterized a mouse model with continuous CT-1 infusion at a clinically relevant concentration of 20 μg/kg/day, which displayed the hallmarks of eccentric hypertrophy after 2 weeks: wall thinning, severe chamber dilation, and a stark reduction in ejection fraction. The CT-1 infusion rodent models may prove useful for future studies examining the biochemical, geometric, or functional ramifications of distinct hypertrophic agonists on the myocardium.

Genetic studies on the involvement of gp130 in cardiac remodeling reveal a requirement of gp130-dependent signaling for myocyte

signaling and either concentric or eccentric remodeling. Data are means ± SEM. One-way ANOVA with Bonferroni's multiple-comparison test was used to compare groups. n, number of hearts; AAV9, adeno-associated vector serotype 9; TAC, transverse aortic constriction; WGA, wheat germ agglutinin; LV mass/BW, left ventricular mass to body weight ratio; LVPWs, left ventricular posterior wall end systole; LVIDs, left ventricular internal diameter in systole; EF, ejection fraction; *Nppa*, natriuretic peptide type A; *Nppb*, natriuretic peptide type B; *Acta1*, alpha skeletal actin; *Myh7*, beta myosin heavy chain. *$p < 0.05$ versus corresponding control group; #$p < 0.05$ versus experimental group.

survival pathways on the one hand, as well as transmitting prohypertrophic signals on the other. Indeed, myocyte-restricted deletion of gp130 yielded massive apoptotic cell death and rapid onset of dilated cardiomyopathy following biomechanical stress.[20] Heart-restricted overexpression of a dominant-negative form of gp130 suppressed many molecular and morphological features of pressure overload-induced concentric hypertrophic remodeling.[21] The molecular decision between survival and hypertrophy is regulated by the interplay between gp130-mediated JAK/STAT activation and suppression of cytokine signaling 1/3 (SOCS1/3), intrinsic JAK inhibitors, and negative feedback regulators for gp130 signaling. AAV transfer of SOCS1 dampened JAK/STAT activation and the transition of hypertrophy to failure in a pressure-overload model *in vivo*.[34] Moreover, adenovirus-mediated gene transfer of SOCS3 to ventricular cardiomyocytes completely suppressed both hypertrophic and antiapoptotic phenotypes in cultured cardiomyocytes induced by LIF.[35] In another study, cardiac-specific SOCS3 knockout mice showed enhanced activation of the signaling targets STAT3, Akt, ERK1/2, and p38 MAPK and spontaneous cardiac eccentric remodeling, occurrence of arrhythmias, and signs of heart failure, all in dependence on the presence of gp130, since SOCS3/gp130 double-knockout mice displayed suppression of the cardiomyopathic phenotype.[36] Further downstream of gp130, a variety of signaling branches are differentially activated by IL-6 cytokines, including the ERK1/2, p38, and ERK5 MAPK terminal branches, JAK/STAT3, PI3K/Akt, Gab1/SHP2, and RhoA.[11,37,38] In line, Mek5 transgenic mice displayed a severe form of eccentric remodeling with wall thinning, chamber dilation, and severe fibrosis,[32] a phenotype that was largely recapitulated by silencing endogenous *miR-148a* using an antagomir strategy in the current study. In contrast, STAT3-deficient mice spontaneously develop signs of injury, inflammation, and cardiac dysfunction with advancing age and in response to cardiac stress.

Accordingly, the prevailing message supports a model where IL-6 cytokine-gp130 confers a level of protective signaling in a variety of cardiac stress conditions and that complete deletion of gp130 signaling components causes widespread cell death. On the other hand, unrestrained activation of cytokine-gp130 signaling also confers prohypertrophic cues that facilitate the transition to eccentric hypertrophy and systolic dysfunction in situations of biomechanical stress. This model of cytokine-gp130 signaling is in line with a regulatory function of cardiac *miR-148a*, where higher *miR-148a* expression and concomitant reduction of gp130 expression sustains the protective cell-survival effects while dampening overactivation of downstream signaling cascades, yielding concentric forms of hypertrophy. With sustained periods of biomechanical stress, decreased *miR-148a* expression and concomitant derepression of gp130 promotes overactivation of a variety of hypertrophic intracellular signals, yielding eccentric hypertrophic remodeling, dilated cardiomyopathy, and systolic dysfunction. As such, the biphasic regulation of *miR-148a* provides a mechanistic explanation for the clinically observed transition from early phase "compensatory" forms of hypertrophy to later phase decompensation and overt heart failure in the setting of sustained biomechanical stress.

MATERIALS AND METHODS

Human Heart Samples

Approval for studies on human tissue samples was obtained from the Medical Ethics Committee of the University Medical Center Utrecht, the Netherlands. All patients or their relatives gave written informed consent before operation, and procedures were compliant with the WMA Declaration of Helsinki and the Department of Health and Human Services Belmont Report. In this study, we included tissue from the left ventricular free wall of patients undergoing heart transplantation with end-stage heart failure and dilated cardiomyopathy (DCM) or hypertrophic cardiomyopathy (HCM). Control tissue was taken from the left ventricular free wall of refused donor hearts that could not be transplanted for technical reasons and where neither donor patient histories nor autopsy revealed signs of heart disease (Table S8).

Mouse Models

Mice used in this study were male and female B6CBAF1 wild-type mice (Charles River Laboratories) of 2–6 months of age. Other mice used in this study were male calcineurin transgenic mice in a B6CBAF1 background expressing an activated mutant of calcineurin in the postnatal heart under control of the 5.5-kb murine *Myh6* promoter (Myh6-CnA[39]). Sample size was determined by a power calculation based on an echocardiographic effect size. Randomization of subjects to experimental groups was based on a single sequence of random assignments. Animal caretakers and investigators were blinded to group allocation during the experiment and/or when assessing the outcome. All protocols were performed according to institutional guidelines and approved by local Animal Care and Use Committees. All mice were housed on a 12-hr:12-hr light:dark cycle in a temperature-controlled environment with *ad libitum* access to water and chow at Innoser Netherlands BV, a commercial mouse-breeding company with a quarterly animal health monitoring system that complies with Federation for Laboratory Animal Science Associations (FELASA) guidelines and recommendations.

Aortic Banding, CT-1 Infusion, and Transthoracic Echocardiography

TAC or sham surgery was performed in 2-month-old wild-type B6CBAF1 female and male mice by subjecting the aorta to a defined 27G constriction between the first and second truncus of the aortic arch, as described previously.[26,40] For Doppler echocardiography, mice were shaved, lightly anaesthetized with isoflurane (mean 1% in oxygen), and allowed to breathe spontaneously through a nasal cone. Non-invasive echocardiography was performed as described previously in detail.[24] Doppler was used to calculate the pressure gradient between the proximal and distal sites of the TAC and only mice with a pressure gradient >50 mm Hg were included. Chronic cardiotrophin 1 (20 μg/kg/day dissolved in PBS), isoproterenol (60 mg/kg/day dissolved in PBS), or saline administration was performed using Alzet miniosmotic pumps (no. 2002; Alza) surgically inserted dorsally and subcutaneously (s.c.) in 2-month-old wild-type B6CBAF1 female and male mice under isoflurane anesthesia and left

for an additional 2 weeks. All protocols were performed according to institutional guidelines and approved by local Animal Care and Use Committees.

Antagomir Studies

Chemically modified antisense oligonucleotides designed to target *mmu-miR-148a-3p* (5′-ACAAAGUUCUGUAGUGCAC-3′/3CholTEG-3′) or *C. elegans miR-39-5p* (5′-AAGGCAAGCUGACCCUGAAGUU-3′/3CholTEG-3′) with a 3′ cholesterol conjugation and two phosphorothioate bonds at the very first 5′ end and four phosphorothioate bonds between the last 3′ bases[41] were synthesized at Integrated DNA Technologies (IDT). All antagomirs were high-performance liquid chromatography (HPLC) purified and desalted before use. Female and male wild-type B6CBAF1 mice (8–10 weeks of age) were subjected to sham or TAC surgery. After 3 days, mice were injected (intraperitoneally) with antagomir-148a (80 mg kg^{-1} BW) or control antagomir (80 mg kg^{-1} BW) for 3 consecutive days. Echo analysis was performed at 3 weeks and 6 weeks after surgery.

AAV Vectors

All of the AAV vectors used in this study were generated by the International Centre for Genetic Engineering and Biotechnology (ICGEB) AAV Vector Unit (AVU) (http://www.icgeb.org/avu-core-facility.html) using a dual-triple plasmid co-transfection procedure followed by polyethylene glycol (PEG) precipitation and purification through CsCl2 gradient centrifugations as described previously.[42] Adult mice were i.v. injected with AAV9-MCS and AAV9-miR-148a via the jugular vein at a dose of 1×10^{12} viral genome particles per animal.

Primary Cardiomyocyte Cultures and Immunocytochemistry

Cardiomyocytes were isolated by enzymatic dissociation of 1- to 2-day-old neonatal rat hearts and processed for immunofluorescence microscopy as described previously.[43] Primary fibroblasts and endothelial cells were obtained from neonatal rat hearts using endothelial and fibroblast isolation kits (Miltenyi Biotec). Neonatal cardiomyocytes were transfected with precursors (Ambion) and inhibitors (Exiqon) of microRNAs (10 nM) using Oligofectamine (Invitrogen). For visualization of cardiomyocyte size and sarcomeric organization, the cells were stained for α2-actinin with mouse monoclonal anti-sarcomeric α-actinin antibody (Sigma-Aldrich, A7811 clone EA-53, 1:500) followed by rat anti-mouse phenylephrine-Texas red-conjugated monoclonal antibody (Life Technologies, RM2817 clone M1/70.15, 1:800). Nuclear staining was performed with VECTASHIELD Mounting Medium (Vector Laboratories) containing DAPI. Myocyte hypertrophy was induced by stimulation for 24 hr with phenylephrine (10 μM) as described previously[43] or with CT-1 (2 nM).

Isolation of Adult Mouse Cardiomyocytes, Fibroblasts, and Endothelial Cells

Cardiomyocytes, fibroblasts, and endothelial cells were isolated from hearts of B6CBAF1 wild-type mice (2- to 6-months-old) following the procedure and the buffer preparations of the Langherdorff-free method previously described.[44] In brief, mice were sacrificed via cervical dislocation; the still-beating heart was fully exposed, isolated from systemic circulation, and perfused once with EDTA buffer through left ventricular injection. Afterward, the heart was transferred into a 60-mm dish and perfused again with new EDTA buffer, moved into a new dish, treated with perfusion buffer, and then serially perfused with collagenase buffer. The tissue was then pulled gently into ~1-mm^3 pieces using forceps and dissociated by pipetting. Stop buffer was added, cell suspension was passed through a strainer, and cardiomyocytes were left to settle for 20 min. Fibroblasts and endothelial cells were separated from the supernatant through Magnetic-activated cell-sorting method.

pMIR-Reporter Assays

Cos7 cells were purchased at the American Type Culture Collection (ATCC; CRL-1651) and cultured in DMEM supplemented with 10% fetal bovine serum (FBS), 100 units/mL penicillin-streptomycin and 2 mmol/L L-glutamine (Thermo Fisher). Cos7 cells were screened for mycoplasma with the MycoAlert PLUS Mycoplasma Detection kit (Lonza) upon receipt from ATCC and subsequently checked on a yearly basis. Cos7 cells were transfected with pMIR reporter plasmids harboring the entire 3′ UTR of mouse gp130, with pMIR reporter plasmids harboring the first part of the 3′ UTR of mouse gp130, or with pMIR reporter plasmids harboring the latter section of the gp130 3′ UTR using X-tremeGENE 9 (Roche) transfection reagent, followed by transfection with *miR-148a* or scrambled miR precursor molecules using Oligofectamine reagent (Invitrogen). Luciferase activity was measured 24 hr after transfection with a dual luciferase assay kit (Promega) using Renilla luciferase as internal control to correct for transfection efficiency.

Northern Blot Analysis

Northern blotting was performed as described previously[24] using 3′-digoxigenin-labeled locked nucleic acid oligonucleotides for *miR-148a* and U6 small nuclear RNA (*Rnu6-2*). Detection was achieved with Fab fragments from polyclonal anti-digoxigenin antibodies, conjugated to alkaline phosphatase (Roche).

Western Blot Analysis

SDS-PAGE electrophoresis and blotting were performed as described previously.[7] Primary antibodies that were used included anti-gp130 (Cell Signaling Technology; rabbit polyclonal antibody [pAb], cat. no. 3732), anti-LIFR (Santa Cruz Biotechnology; mouse monoclonal antibody [mAb], cat sc-515337), anti-CT-1 (Santa Cruz Biotechnology; mouse mAb cline AN-B3, cat. no. sc-9991), anti-GAPDH (Millipore; mouse mAb clone 6C5, cat. no. MAB374), anti-STAT3 (Cell Signaling Technology; mouse mAb clone 124H6, cat. no. 9139), anti-phospho-STAT3 (p-Tyr705) (Cell Signaling Technology; mouse mAb clone M9C6, cat. no. 4113), anti-Akt (Cell Signaling Technology; mouse mAb clone 2H10, cat. no. 2967), anti-phospho-Akt (pSer473) (Cell Signaling Technology; rabbit mAb clone D7F10, cat. no. 9018), anti-p44/42 MAPK (ERK1/2) (Cell Signaling Technology; rabbit mAb clone 137F5, cat. no. 4695), anti-phopsho-p44/42 MAPK (p-Thr202-204-Erk1/2) (Cell Signaling Technology;

rabbit mAb clone D13.14.4E, cat. no. 4370), anti-ERK5 (Cell Signaling Technology rabbit mAb clone D3I5V, cat. no. 12950), anti-phospho-ERK5 (p-Thr218/Tyr220) (Cell Signaling Technology; rabbit pAb, cat. no. 3371) followed by corresponding horseradish peroxidase (HRP)-conjugated secondary antibodies and enhanced chemiluminescence (ECL) detection. Western blots were performed with Stain Free gels for loading control or probed with secondary antibodies: anti-beta-actin (Sigma-Aldrich; mouse mAb, cat. no. A1978-100UL) or anti-tubulin (Sigma-Aldrich mouse mAb, cat. no. T6199-100UL). Signals were detected using the ECL system (Amersham Pharmacia Biotech). Results are expressed as an n-fold increase over the values of the control group in densitometric arbitrary units.

Real-Time qPCR

Total RNA (1 μg) was used in either miR-based or mRNA-based reverse transcription. Real-time PCR was performed on a Bio-Rad iCycler (Bio-Rad) using SYBR Green. Transcript quantities were compared using the relative Ct method, where the amount of target normalized to the amount of endogenous control (L7) and relative to the control sample is given by $2^{-\Delta\Delta Ct}$. For microRNA real-time PCR, miRNAs were isolated with TRIzol reagent (Invitrogen) and cDNA was generated with the miScript Reverse Transcription Kit (QIAGEN). For real-time PCR detection of miRNAs, miScript Primer Assays and the miScript SYBR Green PCR Kit (QIAGEN) were used. Regarding the viral genome copy number assay, total DNA was extracted and used as substrate of the real-time PCR against the Cytomegalovirus (CMV) promoter cloned into the AAV vector genome (primer pair 5′-GGACTTTCCTACTTGGCAGT-3′ and 5′-GTGAGTCAAACCGCTATCCA-3′). A standard curve was obtained by serial dilutions of the AAV plasmid with known concentration. The data were quantified by interpolation with the standard curve, solving the equation for the linear regression Ct = m (log quantity) + b.

microRNA Target Prediction

Putative microRNA-148a target genes were identified using the microRNA databases and target prediction tools miRWalk 2.0 (http://zmf.umm.uni-heidelberg.de/apps/zmf/mirwalk2/index.html), miRBase (https://microrna.sanger.ac.uk/), PicTar (http://pictar.mdc-berlin.de/), and TargetScan (http://targetscan.org/index.html).

Histological Analysis and (Immunofluorescence) Microscopy

Hearts were arrested in diastole, perfusion fixed with 4% paraformaldehyde and PBS solution, embedded in paraffin and sectioned at 4 μm. Paraffin sections were stained with H&E for routine histological analysis; Sirius red for the detection of fibrillar collagen; and fluorescein isothiocyanate (FITC)-labeled wheat-germ-agglutinin (Sigma-Aldrich, 1:100) to visualize and quantify myocyte cross-sectional area. Slides were visualized using a Zeiss Axioskop 2Plus with an AxioCamHRc. Cell surface areas were determined using ImageJ imaging software (http://rsb.info.nih.gov/ij/). Immune cell stainings were performed using rat monoclonal anti-CD45 antibody (Abcam ab23910 IBL-3/16, 1:50) followed by goat anti-rat Alexa Fluor 568-conjugated polyclonal antibody (ThermoFisher, A11077, 1:1000), rabbit polyclonal anti-sarcomeric α-actinin antibody (Abcam, ab137346, 1:100) followed by goat anti-rabbit Alexa Fluor 488-conjugated polyclonal antibody (Thermo Fisher, A11008, 1:1000) and Hoechst 34580 (Thermo Fisher, H21486, 1:1000). TUNEL stainings were performed on 10-μm paraffin sections as described previously in detail[45,46] using a TMR red TUNEL kit (Roche). Double staining was performed with anti-phalloidin-FITC (Sigma,1:500) and/or DAPI (Molecular Probes, 1:500). The samples were examined with a confocal scanning laser microscope Leica TCSNT equipped with argon-krypton and helium-neon lasers.

Statistical Analysis

The results are presented as mean ± SEM. Statistical analyses were performed using Prism software (GraphPad Software), and consisted of ANOVA followed by Bonferroni's multiple-comparison test when group differences were detected at the 5% significance level or Student's t test when comparing two experimental groups. Differences were considered significant when $p < 0.05$. For western blot analysis, normality of distributions was verified by means of the Kolmogorov-Smirnov test. Data were analyzed using ANOVA followed by a Newman-Keuls multiple-comparison test when group differences were detected at the 5% significance level. Differences were considered significant when $p < 0.05$.

SUPPLEMENTAL INFORMATION

Supplemental Information includes five figures and eight tables and can be found with this article online at https://doi.org/10.1016/j.ymthe.2018.11.011.

AUTHOR CONTRIBUTIONS

A.R., E.D., L.E.P., A.F.-C., F.D.M., V.S.-P., M.S., R.J., H.e.A., N.B., S.O., L.Z., and S.Z. performed experiments. A.R. L.E.P., E.D., M.I.F.J.O., P.A.d.C.M., N.L.-A., and L.J.D.W. analyzed data. E.D., L.E.P., P.A.d.C.M., and L.J.D.W. designed the study. M.M.H., R.A.d.W., Y.J.R., Y.M.P., M.G., and N.L.-A. provided reagents, models, or data. A.R., E.D., L.E.P., P.A.d.C.M., N.L.-A., M.C., and L.J.D.W. wrote the manuscript.

CONFLICTS OF INTEREST

P.A.d.C.M. and L.J.D.W. are co-founders and stockholders of Mirabilis Therapeutics BV.

ACKNOWLEDGMENTS

E.D. is supported by VENI award 916-150-16 from the Netherlands Organization for Health Research and Development (ZonMW). V.S.-P. was funded by an individual fellowship (SFRH/BD/11799/2015) from FCT/Ministério da Ciência. P.A.d.C.M. is supported by a MEERVOUD grant from the Netherlands Organisation for Scientific Research (NWO) and is an Established Investigator of the Dutch Heart Foundation. N.L.-A. is supported by Miguel Servet contract CP13/00221 from the "Instituto de Salud Carlos III-FEDER." L.J.D.W. acknowledges support from the Netherlands CardioVascular Research Initiative: the Dutch Heart Foundation,

the Dutch Federation of University Medical Centers, ZonMw, and the Royal Netherlands Academy of Sciences. L.J.D.W. was further supported by grant 311549 from the European Research Council (ERC) and VICI award 918-156-47 from NWO.

REFERENCES

1. Opie, L.H., Commerford, P.J., Gersh, B.J., and Pfeffer, M.A. (2006). Controversies in ventricular remodelling. Lancet *367*, 356–367.
2. Dorn, G.W., 2nd, Robbins, J., and Sugden, P.H. (2003). Phenotyping hypertrophy: eschew obfuscation. Circ. Res. *92*, 1171–1175.
3. Gaasch, W.H., and Zile, M.R. (2011). Left ventricular structural remodeling in health and disease: with special emphasis on volume, mass, and geometry. J. Am. Coll. Cardiol. *58*, 1733–1740.
4. Heineke, J., and Molkentin, J.D. (2006). Regulation of cardiac hypertrophy by intracellular signalling pathways. Nat. Rev. Mol. Cell Biol. *7*, 589–600.
5. Pennica, D., King, K.L., Shaw, K.J., Luis, E., Rullamas, J., Luoh, S.M., Darbonne, W.C., Knutzon, D.S., Yen, R., Chien, K.R., et al. (1995). Expression cloning of cardiotrophin 1, a cytokine that induces cardiac myocyte hypertrophy. Proc. Natl. Acad. Sci. USA *92*, 1142–1146.
6. Wollert, K.C., Taga, T., Saito, M., Narazaki, M., Kishimoto, T., Glembotski, C.C., Vernallis, A.B., Heath, J.K., Pennica, D., Wood, W.I., and Chien, K.R. (1996). Cardiotrophin-1 activates a distinct form of cardiac muscle cell hypertrophy. Assembly of sarcomeric units in series VIA gp130/leukemia inhibitory factor receptor-dependent pathways. J. Biol. Chem. *271*, 9535–9545.
7. López, N., Díez, J., and Fortuño, M.A. (2006). Differential hypertrophic effects of cardiotrophin-1 on adult cardiomyocytes from normotensive and spontaneously hypertensive rats. J. Mol. Cell. Cardiol. *41*, 902–913.
8. Sheng, Z., Pennica, D., Wood, W.I., and Chien, K.R. (1996). Cardiotrophin-1 displays early expression in the murine heart tube and promotes cardiac myocyte survival. Development *122*, 419–428.
9. Brar, B.K., Stephanou, A., Liao, Z., O'Leary, R.M., Pennica, D., Yellon, D.M., and Latchman, D.S. (2001). Cardiotrophin-1 can protect cardiac myocytes from injury when added both prior to simulated ischaemia and at reoxygenation. Cardiovasc. Res. *51*, 265–274.
10. Liao, Z., Brar, B.K., Cai, Q., Stephanou, A., O'Leary, R.M., Pennica, D., Yellon, D.M., and Latchman, D.S. (2002). Cardiotrophin-1 (CT-1) can protect the adult heart from injury when added both prior to ischaemia and at reperfusion. Cardiovasc. Res. *53*, 902–910.
11. López, N., Díez, J., and Fortuño, M.A. (2005). Characterization of the protective effects of cardiotrophin-1 against non-ischemic death stimuli in adult cardiomyocytes. Cytokine *30*, 282–292.
12. López-Andrés, N., Rousseau, A., Akhtar, R., Calvier, L., Iñigo, C., Labat, C., Zhao, X., Cruickshank, K., Díez, J., Zannad, F., et al. (2012). Cardiotrophin 1 is involved in cardiac, vascular, and renal fibrosis and dysfunction. Hypertension *60*, 563–573.
13. Talwar, S., Squire, I.B., Downie, P.F., Davies, J.E., and Ng, L.L. (2000). Plasma N terminal pro-brain natriuretic peptide and cardiotrophin 1 are raised in unstable angina. Heart *84*, 421–424.
14. Talwar, S., Squire, I.B., O'brien, R.J., Downie, P.F., Davies, J.E., and Ng, L.L. (2002). Plasma cardiotrophin-1 following acute myocardial infarction: relationship with left ventricular systolic dysfunction. Clin. Sci. (Lond.) *102*, 9–14.
15. Talwar, S., Squire, I.B., Downie, P.F., O'Brien, R.J., Davies, J.E., and Ng, L.L. (2000). Elevated circulating cardiotrophin-1 in heart failure: relationship with parameters of left ventricular systolic dysfunction. Clin. Sci. (Lond.) *99*, 83–88.
16. Pemberton, C.J., Raudsepp, S.D., Yandle, T.G., Cameron, V.A., and Richards, A.M. (2005). Plasma cardiotrophin-1 is elevated in human hypertension and stimulated by ventricular stretch. Cardiovasc. Res. *68*, 109–117.
17. López, B., González, A., Lasarte, J.J., Sarobe, P., Borrás, F., Díaz, A., Barba, J., Tomás, L., Lozano, E., Serrano, M., et al. (2005). Is plasma cardiotrophin-1 a marker of hypertensive heart disease? J. Hypertens. *23*, 625–632.
18. Zolk, O., Ng, L.L., O'Brien, R.J., Weyand, M., and Eschenhagen, T. (2002). Augmented expression of cardiotrophin-1 in failing human hearts is accompanied by diminished glycoprotein 130 receptor protein abundance. Circulation *106*, 1442–1446.
19. Tsutamoto, T., Wada, A., Maeda, K., Mabuchi, N., Hayashi, M., Tsutsui, T., Ohnishi, M., Fujii, M., Matsumoto, T., Yamamoto, T., et al. (2001). Relationship between plasma level of cardiotrophin-1 and left ventricular mass index in patients with dilated cardiomyopathy. J. Am. Coll. Cardiol. *38*, 1485–1490.
20. Hirota, H., Chen, J., Betz, U.A., Rajewsky, K., Gu, Y., Ross, J., Jr., Müller, W., and Chien, K.R. (1999). Loss of a gp130 cardiac muscle cell survival pathway is a critical event in the onset of heart failure during biomechanical stress. Cell *97*, 189–198.
21. Uozumi, H., Hiroi, Y., Zou, Y., Takimoto, E., Toko, H., Niu, P., Shimoyama, M., Yazaki, Y., Nagai, R., and Komuro, I. (2001). gp130 plays a critical role in pressure overload-induced cardiac hypertrophy. J. Biol. Chem. *276*, 23115–23119.
22. Yoshida, K., Taga, T., Saito, M., Suematsu, S., Kumanogoh, A., Tanaka, T., Fujiwara, H., Hirata, M., Yamagami, T., Nakahata, T., et al. (1996). Targeted disruption of gp130, a common signal transducer for the interleukin 6 family of cytokines, leads to myocardial and hematological disorders. Proc. Natl. Acad. Sci. USA *93*, 407–411.
23. Kunisada, K., Tone, E., Fujio, Y., Matsui, H., Yamauchi-Takihara, K., and Kishimoto, T. (1998). Activation of gp130 transduces hypertrophic signals via STAT3 in cardiac myocytes. Circulation *98*, 346–352.
24. da Costa Martins, P.A., Salic, K., Gladka, M.M., Armand, A.S., Leptidis, S., el Azzouzi, H., Hansen, A., Coenen-de Roo, C.J., Bierhuizen, M.F., van der Nagel, R., et al. (2010). MicroRNA-199b targets the nuclear kinase Dyrk1a in an auto-amplification loop promoting calcineurin/NFAT signalling. Nat. Cell Biol. *12*, 1220–1227.
25. Taga, T., and Kishimoto, T. (1997). Gp130 and the interleukin-6 family of cytokines. Annu. Rev. Immunol. *15*, 797–819.
26. Bourajjaj, M., Armand, A.S., da Costa Martins, P.A., Weijts, B., van der Nagel, R., Heeneman, S., Wehrens, X.H., and De Windt, L.J. (2008). NFATc2 is a necessary mediator of calcineurin-dependent cardiac hypertrophy and heart failure. J. Biol. Chem. *283*, 22295–22303.
27. Dirkx, E., Gladka, M.M., Philippen, L.E., Armand, A.S., Kinet, V., Leptidis, S., El Azzouzi, H., Salic, K., Bourajjaj, M., da Silva, G.J., et al. (2013). Nfat and miR-25 cooperate to reactivate the transcription factor Hand2 in heart failure. Nat. Cell Biol. *15*, 1282–1293.
28. De Windt, L.J., Lim, H.W., Bueno, O.F., Liang, Q., Delling, U., Braz, J.C., Glascock, B.J., Kimball, T.F., del Monte, F., Hajjar, R.J., and Molkentin, J.D. (2001). Targeted inhibition of calcineurin attenuates cardiac hypertrophy in vivo. Proc. Natl. Acad. Sci. USA *98*, 3322–3327.
29. Zacchigna, S., Zentilin, L., and Giacca, M. (2014). Adeno-associated virus vectors as therapeutic and investigational tools in the cardiovascular system. Circ. Res. *114*, 1827–1846.
30. Raso, A., and Dirkx, E. (2017). Cardiac regenerative medicine: At the crossroad of microRNA function and biotechnology. Noncoding RNA Res. *2*, 27–37.
31. Torrado, M., Iglesias, R., Nespereira, B., and Mikhailov, A.T. (2010). Identification of candidate genes potentially relevant to chamber-specific remodeling in postnatal ventricular myocardium. J. Biomed. Biotechnol. *2010*, 603159.
32. Nicol, R.L., Frey, N., Pearson, G., Cobb, M., Richardson, J., and Olson, E.N. (2001). Activated MEK5 induces serial assembly of sarcomeres and eccentric cardiac hypertrophy. EMBO J. *20*, 2757–2767.
33. Kuwahara, K., Saito, Y., Ogawa, Y., Tamura, N., Ishikawa, M., Harada, M., Ogawa, E., Miyamoto, Y., Hamanaka, I., Kamitani, S., et al. (1998). Endothelin-1 and cardiotrophin-1 induce brain natriuretic peptide gene expression by distinct transcriptional mechanisms. J. Cardiovasc. Pharmacol. *31* (*Suppl 1*), S354–S356.
34. Cittadini, A., Monti, M.G., Iaccarino, G., Castiello, M.C., Baldi, A., Bossone, E., Longobardi, S., Marra, A.M., Petrillo, V., Saldamarco, L., et al. (2012). SOCS1 gene transfer accelerates the transition to heart failure through the inhibition of the gp130/JAK/STAT pathway. Cardiovasc. Res. *96*, 381–390.
35. Yasukawa, H., Hoshijima, M., Gu, Y., Nakamura, T., Pradervand, S., Hanada, T., Hanakawa, Y., Yoshimura, A., Ross, J., Jr., and Chien, K.R. (2001). Suppressor of cytokine signaling-3 is a biomechanical stress-inducible gene that suppresses gp130-mediated cardiac myocyte hypertrophy and survival pathways. J. Clin. Invest. *108*, 1459–1467.

36. Yajima, T., Murofushi, Y., Zhou, H., Park, S., Housman, J., Zhong, Z.H., Nakamura, M., Machida, M., Hwang, K.K., Gu, Y., et al. (2011). Absence of SOCS3 in the cardiomyocyte increases mortality in a gp130-dependent manner accompanied by contractile dysfunction and ventricular arrhythmias. Circulation *124*, 2690–2701.

37. Takahashi, N., Saito, Y., Kuwahara, K., Harada, M., Tanimoto, K., Nakagawa, Y., Kawakami, R., Nakanishi, M., Yasuno, S., Usami, S., et al. (2005). Hypertrophic responses to cardiotrophin-1 are not mediated by STAT3, but via a MEK5-ERK5 pathway in cultured cardiomyocytes. J. Mol. Cell. Cardiol. *38*, 185–192.

38. Fahmi, A., Smart, N., Punn, A., Jabr, R., Marber, M., and Heads, R. (2013). p42/p44-MAPK and PI3K are sufficient for IL-6 family cytokines/gp130 to signal to hypertrophy and survival in cardiomyocytes in the absence of JAK/STAT activation. Cell. Signal. *25*, 898–909.

39. Molkentin, J.D., Lu, J.R., Antos, C.L., Markham, B., Richardson, J., Robbins, J., Grant, S.R., and Olson, E.N. (1998). A calcineurin-dependent transcriptional pathway for cardiac hypertrophy. Cell *93*, 215–228.

40. Rockman, H.A., Ross, R.S., Harris, A.N., Knowlton, K.U., Steinhelper, M.E., Field, L.J., Ross, J., Jr., and Chien, K.R. (1991). Segregation of atrial-specific and inducible expression of an atrial natriuretic factor transgene in an in vivo murine model of cardiac hypertrophy. Proc. Natl. Acad. Sci. USA *88*, 8277–8281.

41. Krützfeldt, J., Rajewsky, N., Braich, R., Rajeev, K.G., Tuschl, T., Manoharan, M., and Stoffel, M. (2005). Silencing of microRNAs in vivo with 'antagomirs'. Nature *438*, 685–689.

42. Arsic, N., Zentilin, L., Zacchigna, S., Santoro, D., Stanta, G., Salvi, A., Sinagra, G., and Giacca, M. (2003). Induction of functional neovascularization by combined VEGF and angiopoietin-1 gene transfer using AAV vectors. Mol. Ther. *7*, 450–459.

43. De Windt, L.J., Lim, H.W., Haq, S., Force, T., and Molkentin, J.D. (2000). Calcineurin promotes protein kinase C and c-Jun NH2-terminal kinase activation in the heart. Cross-talk between cardiac hypertrophic signaling pathways. J. Biol. Chem. *275*, 13571–13579.

44. Ackers-Johnson, M., Li, P.Y., Holmes, A.P., O'Brien, S.M., Pavlovic, D., and Foo, R.S. (2016). A Simplified, Langendorff-Free Method for Concomitant Isolation of Viable Cardiac Myocytes and Nonmyocytes From the Adult Mouse Heart. Circ Res. *119*, 909–920.

45. Kostin, S., Pool, L., Elsässer, A., Hein, S., Drexler, H.C., Arnon, E., Hayakawa, Y., Zimmermann, R., Bauer, E., Klövekorn, W.P., and Schaper, J. (2003). Myocytes die by multiple mechanisms in failing human hearts. Circ. Res. *92*, 715–724.

46. van Empel, V.P., Bertrand, A.T., van der Nagel, R., Kostin, S., Doevendans, P.A., Crijns, H.J., de Wit, E., Sluiter, W., Ackerman, S.L., and De Windt, L.J. (2005). Downregulation of apoptosis-inducing factor in harlequin mutant mice sensitizes the myocardium to oxidative stress-related cell death and pressure overload-induced decompensation. Circ. Res. *96*, e92–e101.

YMTHE, Volume *27*

Supplemental Information

Therapeutic Delivery of miR-148a Suppresses Ventricular Dilation in Heart Failure

Andrea Raso, Ellen Dirkx, Leonne E. Philippen, Amaya Fernandez-Celis, Federica De Majo, Vasco Sampaio-Pinto, Marida Sansonetti, Rio Juni, Hamid el Azzouzi, Martina Calore, Nicole Bitsch, Servé Olieslagers, Martinus I.F.J. Oerlemans, Manon M. Huibers, Roel A. de Weger, Yolan J. Reckman, Yigal M. Pinto, Lorena Zentilin, Serena Zacchigna, Mauro Giacca, Paula A. da Costa Martins, Natalia López-Andrés, and Leon J. De Windt

Supplemental Figure 1

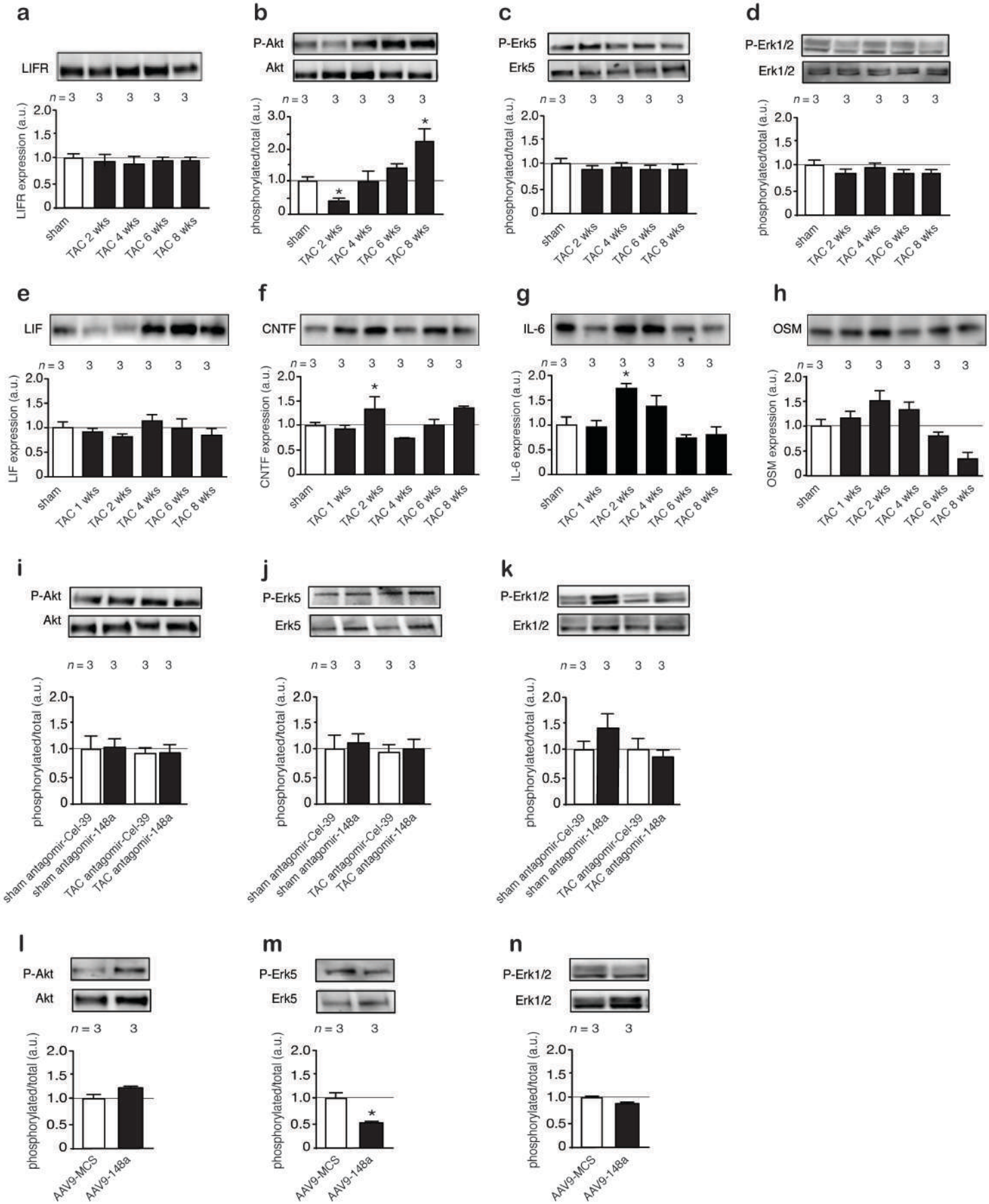

Supplemental Figure 2

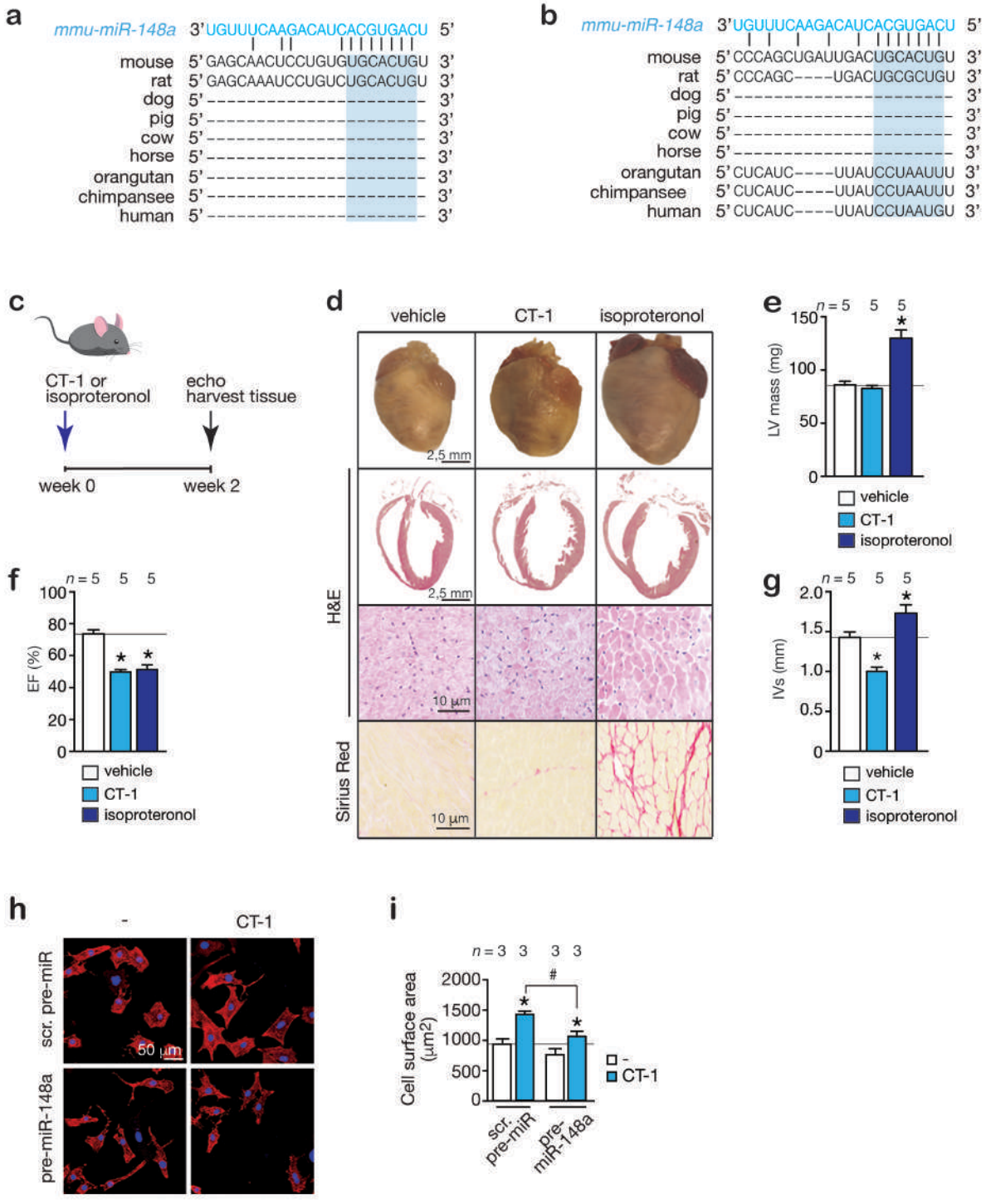

Supplemental Figure 3

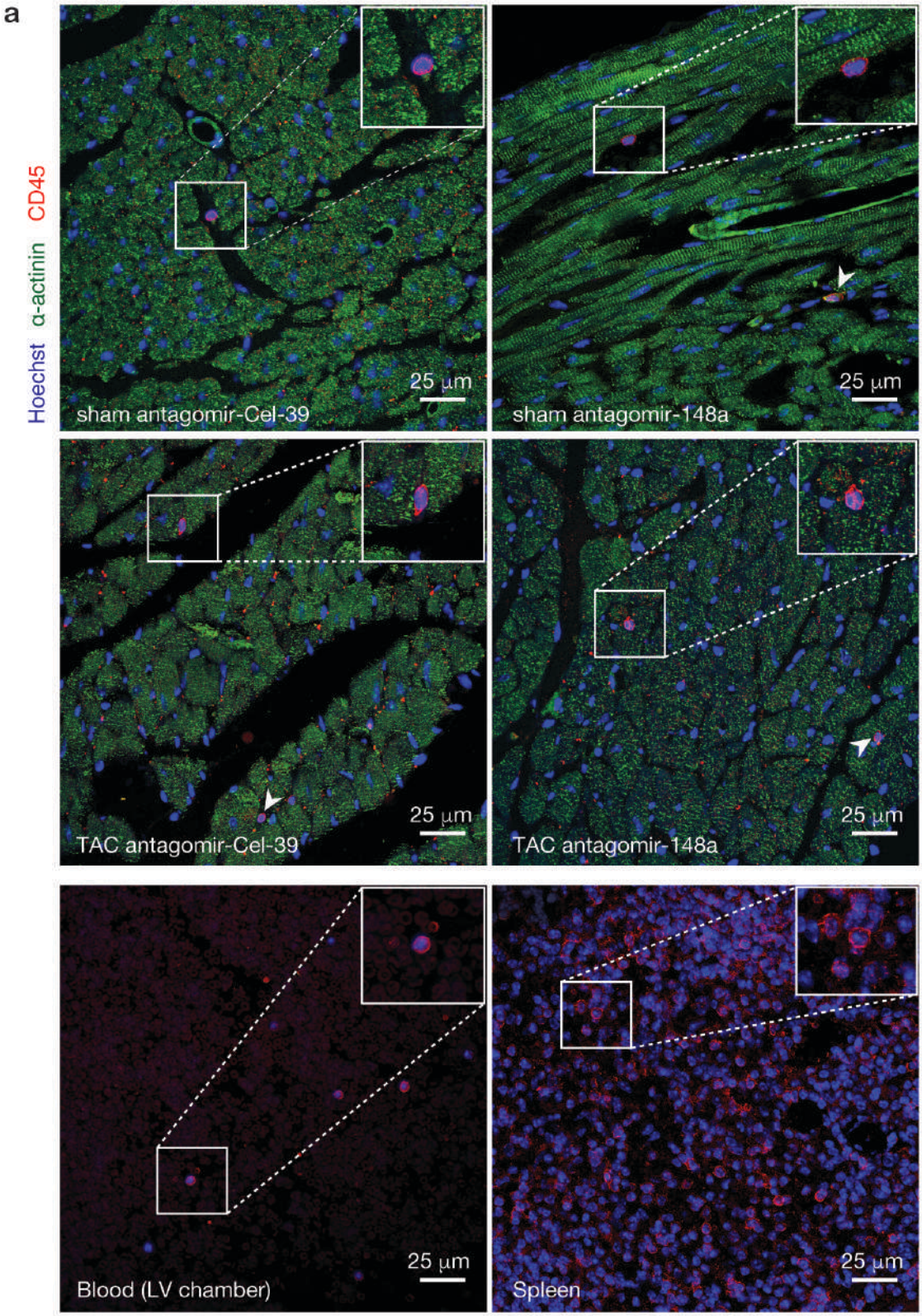

Supplemental Figure 4

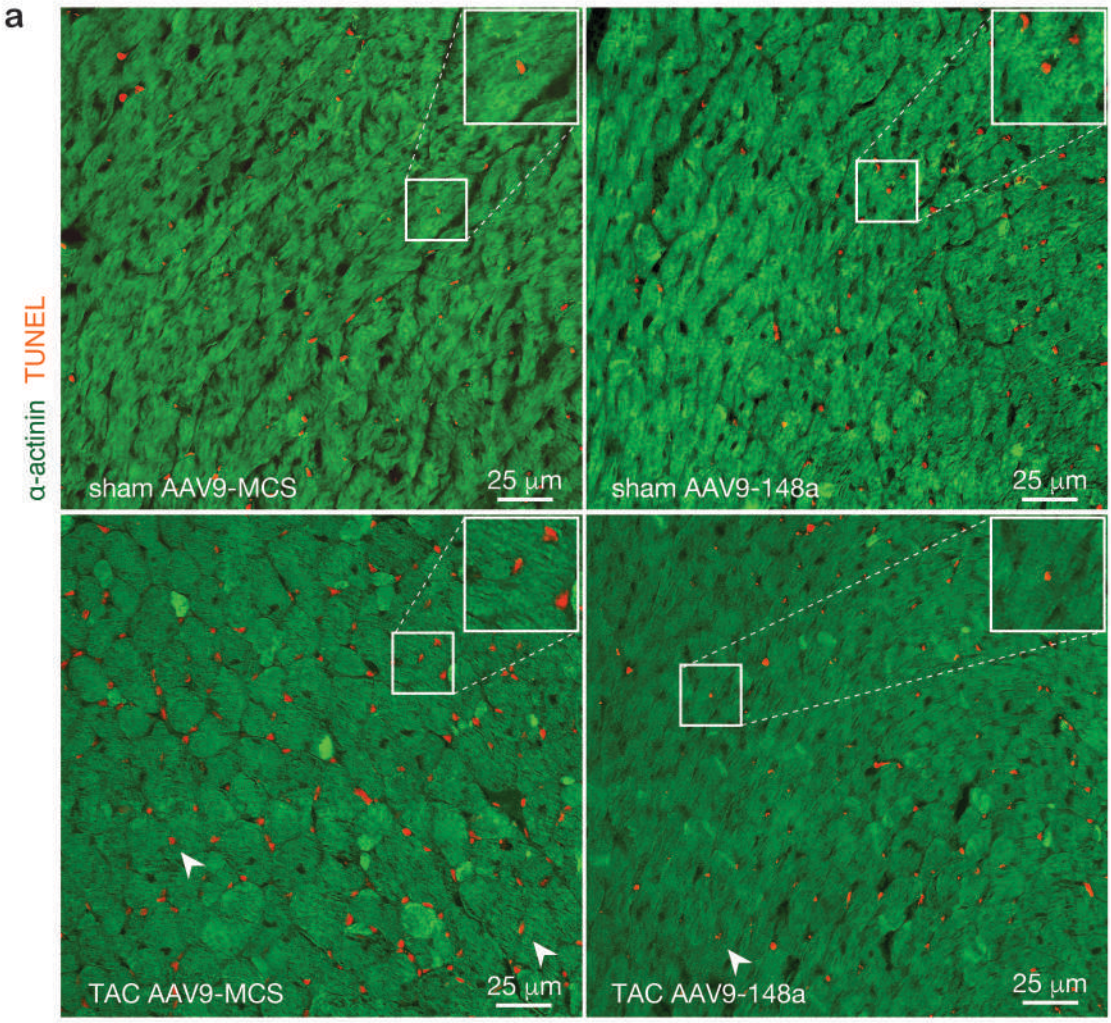

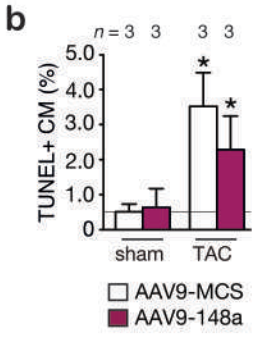

Supplemental Figure 5

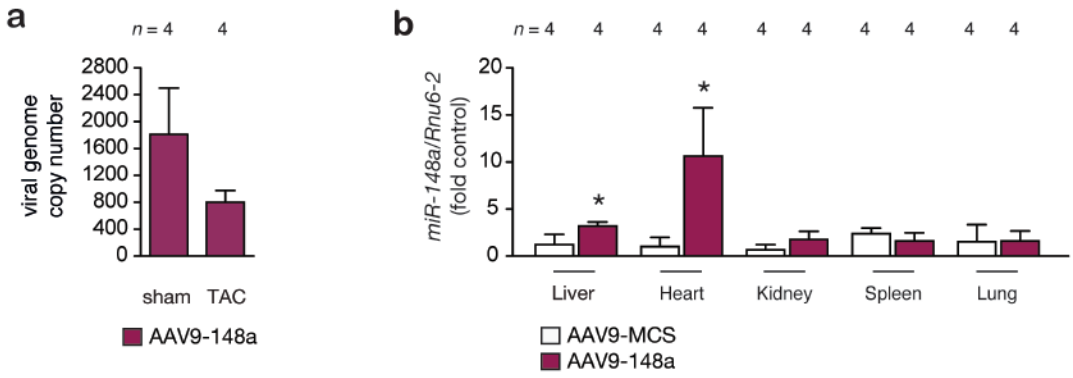

Legends to the Supplementary Figures

Supplementary Figure 1 | *miR-148a* differentially regulates ERK5, ERK1/2, Akt downstream signaling in concentric and eccentric cardiac remodeling. **(a)** Western blot analysis of myocardial LIFR expression and quantification at indicated time points. **(b-d)** Western blot analysis of phosphorylated and unphosphorylated forms of Akt, Erk5 or Erk1/2 and quantification at indicated time points. **(e-h)** Western blot analysis of myocardial LIF, CNTF, IL-6 or OSM expression and quantification at indicated time points. **(i-k)** Western blot analysis of phosphorylated and unphosphorylated forms of Akt, Erk5 or Erk1/2 and quantification in hearts from mice subjected to sham or TAC surgery and receiving antagomir-148a or a control antagomir (antagomir-*Cel*-39). **(l-n)** Western blot analysis of myocardial gp130 or phosphorylated and unphosphorylated forms of Akt, Erk5 or Erk1/2 and quantification in hearts from mice receiving AAV9-148a or AAV9-MCS.

Data information: Data are means ± SEM. One-way ANOVA with Newman-Keuls multiple comparison test was used to compare groups. *n*, number of independent WB experiments; AAV9, adeno-associated virus serotype 9*;* TAC, transverse aortic constriction. *$P < 0.05$ vs corresponding control group.

Supplementary Figure 2 | CT-1 infusion results in cardiac dilation. (a-b) Evolutionary conservation of the other two *mmu-miR-148a* seed regions on gp130 3'UTR. In mouse they are respectively located on the nucleotide position 6150-6156 and 8532-8538 [ENSMUST00000183663.7]. **(c)** Study design of mice receiving continuous infusion of CT-1 (20 µg/kg/day) or isoproterenol (60 mg/kg/day). **(d)** Representative image of whole hearts (top panels), H&E-stained cardiac sections (second panels), high magnification H&E-stained sections (third panels), or Sirius Red stained (lower panels) histological sections of hearts from saline, CT-1 infused and isoproterenol-infused mice. Measurements of **(e)** LV mass, **(f)** EF **(g)** IVSs in saline, CT-1-treated or isoproterenol-treated mice. **(h)** Confocal microscopy images of neonatal rat cardiomyocytes treated with scrambled or precursor-148a miR-148a with or without CT-1 stimulation. **(i)** Cell surface measurements from conditions in (**f**).

Data information: Data are means ± SEM. One-way ANOVA with Bonferonni's multiple comparison test was used to compare groups. *n*, number of mice CT-1, cardiotrophin 1;

LV, left ventricular; EF, ejection fraction; IVSs, Interventricular septum in systole. *$P < 0.05$ vs corresponding control group; #$P < 0.05$ vs experimental group.

Supplementary Figure 3 | Immune response in hearts from mice with altered *miR-148a* expression. (a) Representative confocal images of CD45 labeling in hearts after sham-operation or aortic banding in the presence of control antagomir targeting *C. elegans miR-39* (antagomir-*Cel-39*) or antagomir against *mmu-miR-148a-3p* (top and second panel), with CD45 positive cells (red), cardiomyocytes visualized with sarcomeric actin (green) and nuclei visualized with Hoechst (blue). Blood clot into the left ventricular chamber (left-bottom panel) and spleen (right-bottom panel) were used as internal and external staining positive controls.

Supplementary Figure 4 | Apoptotic events in hearts from mice with altered *miR-148a* expression. (a) Representative confocal images of TUNEL labeling in hearts after sham-operation or aortic banding in the presence of AAV9-MCS or AAV9-148a, with TUNEL positive nuclei (red) and cardiomyocytes visualized with sarcomeric actin (green). **(b)** Quantification of TUNEL positive cardiomyocytes in experimental groups demonstrates a higher percentage of TUNEL positive myocytes after TAC compared to sham.
Data information: Data are means ± SEM. One-way ANOVA with Bonferroni's multiple comparison test was used to compare groups. *n*, number of mice; AAV9, adeno-associated virus; MCS, multiple cloning site; TAC, transverse aortic constriction. *$P < 0.05$ vs corresponding control group.

Supplementary Figure 5 | Characterization of AAV9 transduction treatment. (a) RT-PCR analysis of viral genome copy numbers in 20ng of total DNA in hearts from mice receiving AAV9-148a virus. **(b)** RT-PCR analysis of *miR-148a-3p* expression in diverse organs from mice receiving AAV9-MCS or AAV9-148a virus.
Data information: Data are means ± SEM. One-way ANOVA with Bonferroni's multiple comparison test was used to compare groups. *n*, number of mice; AAV9, adeno-associated virus; MCS, multiple cloning site. *$P < 0.05$ vs corresponding control group.

Supplemental Table 1. Morphometric and echocardiographic characteristics of mice subjected to sham or TAC surgery and treated for 3 weeks with control (Ctrl) antagomir or antagomir-148a.

	Sham		TAC	
	Ctrl antagomir	Antagomir-148a	Ctrl antagomir	Antagomir-148a
n	5	5	8	8
BW (g)	22.8±2.1	25.3±2.0	23.8±1.5	24.3±1.7
LV mass (mg)	73±1	104±18*	120±19*	121±26*
LV mass/BW (mg/g)	3.2±0.2	3.8±0.4	5.2±0.4*	6.4±1.0*
IVSd (mm)	0.87±0.03	0.84±0.06	0.89±0.14	0.87±0.13
IVSs (mm)	1.42±0.01	1.33±0.10	1.03±0.16*	1.17±0.17
LVIDd (mm)	3.39±0.10	3.57±0.25	3.66±0.54	3.62±0.57
LVIDs (mm)	2.06±0.16	2.49±0.26	2.76±0.43*	2.78±0.50*
LVPWd (mm)	0.76±0.06	1.08±0.12*	0.87±0.15	0.86±0.14
LVPWs (mm)	1.12±0.09	1.18±0.15	0.96±0.14	1.07±0.16
EF (%)	77±4	66±5*	57±3*	56±5*
FS (%)	39±3	31±3*	25±2*	25±3*
E/A (mm/s)	1.16±0.04	1.23±0.08	1.65±0.13*	1.57±0.24*

Data are expressed as means ± SEM. BW, body weight; LV, left ventricular; IVSd, interventricular septal thickness at end-diastole; IVSs, interventricular septal thickness at end-systole; LVIDd, left ventricular internal dimension at end-diastole; LVIDs, left ventricular internal dimension at end-systole; LVPwd, left ventricular posterior wall thickness at end-diastole; LVPws, left ventricular posterior wall thickness at end-systole; EF, ejection fraction; FS, fractional shortening; E/A, Doppler E/A ratio. *, indicates $P<0.05$ vs sham group subjected to treatment with a control antagomir; #, indicates $P<0.05$ vs experimental group.

Supplemental Table 2. Morphometric and echocardiographic characteristics of mice subjected to sham or TAC surgery and treated for 6 weeks with control (Ctrl) antagomir or antagomir-148a.

	Sham		TAC	
	Ctrl antagomir	Antagomir-148a	Ctrl antagomir	Antagomir-148a
n	7	8	8	8
BW (g)	22.5±1.6	25.6±1.6	25.6±1.2	24.0±1.6
LV mass (mg)	84±3	77±11	135±26*	135±20
LV mass/BW (mg/g)	3.8±0.3	4.0±0.2	4.8±0.4*	6.1±0.5*
IVSd (mm)	0.87±0.03	0.72±0.05	0.88±0.05	1.00±0.04
IVSs (mm)	1.39±0.05	1.08±0.10*	1.13±0.06	1.22±0.11
LVIDd (mm)	3.44±0.07	3.93±0.34	4.06±0.29	4.47±0.21*
LVIDs (mm)	2.07±0.16	2.90±0.36	2.97±0.33*	3.62±0.25*
LVPWd (mm)	0.89±0.03	0.69±0.04	1.04±0.12	0.85±0.08
LVPWs (mm)	1.28±0.09	0.94±0.09	1.33±0.11	1.00±0.11
EF (%)	78±4	59±6*	61±4*	47±4*
FS (%)	40±4	27±4*	27±2*	20±2*
E/A (mm/s)	1.33±0.13	1.32±0.17	1.52±0.17	1.27±0.04

Data are expressed as means ± SEM. BW, body weight; Ctrl, control; LV, left ventricular; IVSd, interventricular septal thickness at end-diastole; IVSs, interventricular septal thickness at end-systole; LVIDd, left ventricular internal dimension at end-diastole; LVIDs, left ventricular internal dimension at end-systole; LVPwd, left ventricular posterior wall thickness at end-diastole; LVPws, left ventricular posterior wall thickness at end-systole; EF, ejection fraction; FS, fractional shortening; E/A, Doppler E/A ratio; TAC, transverse aortic constriction. *, indicates $P<0.05$ vs sham group subjected to treatment with a control antagomir; #, indicates $P<0.05$ vs experimental group.

Supplemental Table 3. Morphometric and echocardiographic characteristics of mice subjected to sham or TAC surgery and treated with AAV9-MCS or AAV9-miR-148a for 3 weeks.

	Sham		TAC	
	AAV9-MCS	AAV9-miR148a	AAV9-MCS	AAV9-miR148a
n	8	5	10	14
BW (g)	20.8±0.6	21.6±1.4	20.5±2.3	24.0±0.7
LV mass (mg)	69±6	77±6	125±10*	118±6*
LV mass/BW (mg/g)	3.3±0.03	3.6±1.8	5.7±0.56*	5.0±0.22*
IVSd (mm)	0.75±0.03	0.81±0.04	0.94±0.06*	0.94±0.04*
IVSs (mm)	1.13±0.04	1.19±0.05	1.24±0.07	1.33±0.04*
LVIDd (mm)	3.61±0.10	3.67±0.10	4.07±0.12*	3.98±0.06*
LVIDs (mm)	2.47±0.10	2.54±0.10	3.10±0.17*	2.97±0.11*
LVPWd (mm)	0.68±0.06	0.72±0.03	0.97±0.05	0.96±0.03*
LVPWs (mm)	1.03±0.05	1.03±0.02	1.24±0.05*	1.25±0.03*
EF (%)	67±2	69±1	53±5*	58±3*
FS (%)	31±1	31±1	23±2*	26±2*

Data are expressed as means ± SEM. AAV, adeno-associated virus; BW, body weight; LV, left ventricular; IVSd, interventricular septal thickness at end-diastole; IVSs, interventricular septal thickness at end-systole; LVIDd, left ventricular internal dimension at end-diastole; LVIDs, left ventricular internal dimension at end-systole; LVPwd, left ventricular posterior wall thickness at end-diastole; LVPws, left ventricular posterior wall thickness at end-systole; EF, ejection fraction; FS, fractional shortening; MCS, multiple cloning site; TAC, transverse aortic constriction. *, indicates $P<0.05$ vs AAV-MCS sham group; #, indicates $P<0.05$ vs experimental group.

Supplemental Table 4. Morphometric and echocardiographic characteristics of mice subjected to sham or TAC surgery and treated with AAV9-MCS or AAV9-miR-148a for 6 weeks.

	Sham		TAC	
	AAV9-MCS	AAV9-miR148a	AAV9-MCS	AAV9-miR148a
n	11	10	10	14
BW (g)	19.1±0.5	23.8±1.0	22.6±1.2	25.1±0.9
LV mass (mg)	82±3	99±8	102±7*	116±5*
LV mass/BW (mg/g)	3.9±0.1	4.1±0.2	4.6±0.4*	4.6±0.2*
IVSd (mm)	0.84±0.02	0.93±0.02*	0.85±0.02	0.91±0.02*#
IVSs (mm)	1.21±0.05	1.39±0.03*	1.17±0.05	1.26±0.03
LVIDd (mm)	3.57±0.07	3.58±0.08	4.06±0.14*	4.09±0.08*
LVIDs (mm)	2.27±0.10	2.22±0.09	3.23±0.19*	3.08±0.11*
LVPWd (mm)	0.82±0.02	0.95±0.10	0.79±0.03*	0.92±0.02#
LVPWs (mm)	1.23±0.03	1.38±0.09	1.00±0.04*	1.22±0.03#
EF (%)	74±2	76±2	46±5*	57±3*#
FS (%)	37±2	38±2	19±2*	26±2*#
E/A (mm/s)	1.24±0.04	1.25±0.05	1.35±0.03	1.19±0.02

Data are expressed as means ± SEM. AAV, adeno-associated virus; BW, body weight; LV, left ventricular; IVSd, interventricular septal thickness at end-diastole; IVSs, interventricular septal thickness at end-systole; LVIDd, left ventricular internal dimension at end-diastole; LVIDs, left ventricular internal dimension at end-systole; LVPwd, left ventricular posterior wall thickness at end-diastole; LVPws, left ventricular posterior wall thickness at end-systole; EF, ejection fraction; FS, fractional shortening; E/A, Doppler E/A ratio; MCS, multiple cloning site; TAC, transverse aortic constriction. *, indicates $P<0.05$ vs AAV-MCS sham group; #, indicates $P<0.05$ vs experimental group.

Supplemental Table 5. Morphometric and echocardiographic characteristics of mice subjected to sham or TAC surgery for 3 weeks, before treatment with AAV9-MCS or AAV9-miR-148a at 4 weeks after surgery.

	Sham		TAC	
	AAV9-MCS	AAV9-miR148a	AAV9-MCS	AAV9-miR148a
n	9	10	10	11
BW (g)	21.1±0.18	21.2±0.3	19.4±0.3	19.5±0.4
LV mass (mg)	79±3	85±4	97±3*	101±5*
LV mass/BW (mg/g)	3.7±0.12	4.0±0.22	5.0±0.17*	5.2±0.25*
IVSd (mm)	0.68±0.02	0.71±0.08	0.90±0.03*	0.94±0.03*
IVSs (mm)	0.99±0.04	1.05±0.10	1.23±0.04*	1.32±0.05*
LVIDd (mm)	3.31±0.06	3.39±0.34	3.69±0.06*	3.72±0.06*
LVIDs (mm)	2.14±0.06	2.15±0.21	2.59±0.05*	2.59±0.11*
LVPWd (mm)	0.72±0.04	0.77±0.09	0.92±0.02*	0.90±0.06*
LVPWs (mm)	1.03±0.02	1.08±0.10	1.22±0.03*	1.20±0.06*
EF (%)	73±2	74±3	65±2*	65±3*
FS (%)	35±1	37±2	30±2*	30±3*

Data are expressed as means ± SEM. AAV, adeno-associated virus; BW, body weight; LV, left ventricular; IVSd, interventricular septal thickness at end-diastole; IVSs, interventricular septal thickness at end-systole; LVIDd, left ventricular internal dimension at end-diastole; LVIDs, left ventricular internal dimension at end-systole; LVPwd, left ventricular posterior wall thickness at end-diastole; LVPws, left ventricular posterior wall thickness at end-systole; EF, ejection fraction; FS, fractional shortening; MCS, multiple cloning site; TAC, transverse aortic constriction. *, indicates $P<0.05$ vs AAV-MCS sham group; #, indicates $P<0.05$ vs experimental group.

Supplemental Table 6. Morphometric and echocardiographic characteristics of 3 weeks sham and TAC surgery followed by a 1 week post-treatment with AAV-MCS or AAV9-miR-148a.

	Sham		TAC	
	AAV9-MCS	**AAV9-miR148a**	**AAV9-MCS**	**AAV9-miR148a**
n	9	10	10	11
BW (g)	21.2±0.22	21.3±0.35	20.7±0.47	20.91±0.34
LV mass (mg)	80.5±4	89.2±3	101±7*	102±5*
LV mass/BW (mg/g)	3.7±0.16	4.2±0.13	4.7±0.25*	4.9±0.27*
IVSd (mm)	0.73±0.03	0.78±0.03	0.83±0.04*	0.89±0.04*
IVSs (mm)	1.19±0.04	1.10±0.03	1.14±0.04	1.22±0.03*
LVIDd (mm)	3.83±0.04	3.91±0.09	4.03±0.08*	3.91±0.07*
LVIDs (mm)	2.52±0.06	2.75±0.11	3.14±0.10*	2.88±0.09*^
LVPWd (mm)	0.78±0.04	0.81±0.04	0.85±0.06	0.87±0.05
LVPWs (mm)	1.11±0.03	1.13±0.56	1.02±0.05	1.18±0.04^
EF (%)	72±2	65±9	53±2*	59±3*
FS (%)	34±1	30±2	23±2*	26±2*

Data are expressed as means ± SEM. AAV, adeno-associated virus; BW, body weight; LV, left ventricular; IVSd, interventricular septal thickness at end-diastole; IVSs, interventricular septal thickness at end-systole; LVIDd, left ventricular internal dimension at end-diastole; LVIDs, left ventricular internal dimension at end-systole; LVPwd, left ventricular posterior wall thickness at end-diastole; LVPws, left ventricular posterior wall thickness at end-systole; EF, ejection fraction; FS, fractional shortening; TAC, transverse aortic constriction. *, indicates $P<0.05$ vs AAV-MCS sham group; #, indicates $P<0.05$ vs experimental group.

Supplemental Table 7. Morphometric and echocardiographic characteristics of mice subjected to 7 weeks of sham or TAC surgery and treated AAV9-MCS or AAV9-miR-148a for 3 weeks.

	Sham		TAC	
	AAV9-MCS	AAV9-miR148a	AAV9-MCS	AAV9-miR148a
n	9	10	10	11
BW (g)	22.0±0.3	22.0±0.5	21.2±0.3	22.0±0.5
LV mass (mg)	88±4	86±3	105±6*	116±5*
LV mass/BW (mg/g)	4.0±0.2	3.9±0.1	4.8±0.3*	5.3±0.3*
IVSd (mm)	0.73±0.03	0.79±0.04	0.83±0.05*	0.90±0.03*
IVSs (mm)	1.07±0.03	1.07±0.06	1.15±0.05	1.20±0.04*
LVIDd (mm)	3.85±0.04	3.79±0.06	4.20±0.10*	4.02±0.08*
LVIDs (mm)	2.62±0.04	2.59±0.08	3.31±0.15*	2.90±0.08*#
LVPWd (mm)	0.89±0.08	0.84±0.04	0.80±0.05	0.94±0.05#
LVPWs (mm)	1.17±0.05	1.13±0.04	1.01±0.06	1.23±0.05#
EF (%)	70±2	68±9	50±4*	61±2*#
FS (%)	32±1	31±2	21±2*	27±1#

Data are expressed as means ± SEM. AAV, adeno-associated virus; BW, body weight; LV, left ventricular; IVSd, interventricular septal thickness at end-diastole; IVSs, interventricular septal thickness at end-systole; LVIDd, left ventricular internal dimension at end-diastole; LVIDs, left ventricular internal dimension at end-systole; LVPwd, left ventricular posterior wall thickness at end-diastole; LVPws, left ventricular posterior wall thickness at end-systole; EF, ejection fraction; FS, fractional shortening; MCS, multiple cloning site; TAC, transverse aortic constriction. *, indicates $P<0.05$ vs AAV-MCS sham group; #, indicates $P<0.05$ vs experimental group.

Supplemental Table 8. Patient and donor characteristics.

	Gender	Age at Htx (yrs)	LVAD	LVEF (%)	LV ED/ES (mm)	LV PWT (mm)
DCM 1	female	48	yes	10	68/65	7
DCM 2	male	55	no	20	69/65	8
DCM 3	male	57	yes	15	47/43	10
DCM 4	male	47	no	25	51/49	10
DCM 5	male	66	no	25	58/54	10
DCM 6	female	21	yes	15	61/54	6
DCM 7	female	58	yes	15	65/57	8
DCM 8	male	36	yes	15	69/63	8
DCM 9	female	58	yes	20	67/62	6
DCM 10	male	61	yes	10	62/60	7
HCM 1	male	57	no	55	43/42	16
HCM 2	male	31	no	15	85/81	13
HCM 3	male	37	no	20	66/54	13
HCM 4	male	36	no	25	47/39	15
HCM 5	female	31	no	50	29/10	18
HCM 6	female	36	no	40	45/20	14
HCM 7	male	25	no	45	40/20	20
HCM 8	female	36	no	45	45/28	15
HCM 9	female	34	no	20	52/40	13
Control 1	-	-	no	-	-	-
Control 2	-	-	no	-	-	-
Control 3	male	65	no	-	-	-
Control 4	female	72	no	-	-	-
Control 5	male	39	no	-	-	-
Control 6	female	48	no	-	-	-
Control 7	male	38	no	-	-	-
Control 8	female	53	no	-	-	-
Control 9	male	32	no	-	-	-
Control 10	male	43	no	-	-	-
Control 11	male	48	no	-	-	-

DCM, dilated cardiomyopathy; HCM, hypertrophic cardiomyopathy; LVAD, patient received left ventricular assist device; LVEF, left ventricular ejection fraction; LV ED, left ventricular end-diastolic dimension; LV ES, left ventricular end-systolic dimenstion; LVPWT, left ventricular posterior wall thickness; yrs, years; mm, millimeter; -, information not available,.